PEOPLE'S DEMOCRATIC REPUBLIC OF ALGERIA

Ministry of Higher Education and Scientific Research

SAAD DAHLEB University – BLIDA 1

Faculty of Technology

Department of Water and Environmental Sciences

Master's Thesis

Field of Study: Hydraulics

Specialty: Water Resources

Topic

Numerical Simulation of Flooding and Hydraulic Risk Assessment in the Wadi El Hamiz Region

Realized by:

Chouki Idriss Grinou

Proposed by :

Dr. Ahcene Bouach

Presented in front the jury composed of:

Dr. Merabti, A	Associate Professor	Univ. Blida 1	President
Dr. Benzinebe, K	Associate Professor	Univ. Blida 1	Examiner
Dr. Bouach, A	Associate Professor	Univ. Blida 1	Supervisor

June 2025

Dedication

I dedicate this modest work:

To my parents, **Aissa** and **Wahiba**, who have been my source of inspiration and motivation.
Their smiles are the reason I keep moving forward.

No tribute could ever match the love and support they have given me.
May God bless them with good health and long life.

To my close friends, who have become my family over time.

Thank you for everything.

Acknowledgments

First and foremost, we would like to express our sincere gratitude to our supervisor, **Dr. Ahcene Bouach.**, for having accepted to guide this work and for his constant support and encouragement throughout its completion.

I hope these few words convey the depth of our appreciation.

I also extend my thanks to the jury members, **Dr. Merabti**, **A.** for agreeing to chair the jury, and **Dr. Benzineb**e **K**. for accepting to examine my work.

Finally, I would like to warmly thank all my friends, my family members, and everyone who, in one way or another, contributed to the completion of this modest work.

ملخص

تتمحور هذه المذكرة حول تحليل ومحاكاة خطر الفيضانات داخل حوض وادي الحميز .تمثّل الهدف الأساسي في تقييم مدى هشاشة المنطقة المدروسة أمام الفيضانات وتحديد المناطق الأكثر عرضة للخطر، وذلك من خلال النمذجة الرقمية .ولتحقيق ذلك، تم استخدام برنامج HEC-RAS لمحاكاة جريان المياه وانتشار الفيضانات، اعتمادًا على بيانات طبوغرافية وهيدرولوجية واقعية .و م اعتماد سيناريو فيضان لتحليل ارتفاعات المياه وسرعات الجريان داخل الحوض .أظهرت الدراسة فعالية النمذجة الهيدروليكية في تقييم مخاطر الفيضانات، وقدمت نتائج قيمة يمكن الاستفادة منها في التخطيط العمراني والوقاية من الكوارث .وعلى الرغم من بعض القيود المتعلقة بتوفر البيانات وبعض تبسيطات النموذج، فإن هذا العمل يبرز أهمية دمج الأدوات العلمية في استراتيجيات إدارة المخاطر الطبيعية.

لكلمات المفتاحية :خطر الفيضانات، النمذجة الرقمية، المحاكاة الهيدروليكية، الحوض المائي.

Abstract

This master's project focuses on the analysis and simulation of flood risks within the El-Hamiz watershed. The objective was to assess the vulnerability of the study area to flooding events and to identify the high-risk zones through numerical modeling. To achieve this, the HEC-RAS software was used to simulate water flow and flood propagation based on real terrain and hydrological data. A flood scenario was considered for analysis of water levels and flow velocities across the basin. The study demonstrated the effectiveness of using hydraulic modeling in flood risk assessment and provided valuable insights into the behavior of the river system under extreme hydrological conditions. The results can serve as a decision-making tool for territorial planning and risk prevention. Despite some limitations related to data availability and model assumptions, this work highlights the importance of integrating scientific tools into natural hazard management strategies.

Keywords: Flood Risk, Numerical Modeling, Hydraulic Simulation, HEC-RAS, Watershed.

Résumé

Ce mémoire porte sur l'analyse et la simulation du risque d'inondation au sein du bassin versant de l'Oued El-Hamiz. L'objectif principal a été d'évaluer la vulnérabilité de la zone d'étude face aux crues et d'identifier les secteurs à risque à travers une modélisation numérique. Pour ce faire, le logiciel **HEC-RAS** a été utilisé afin de simuler l'écoulement de l'eau et la propagation des inondations, à partir de données topographiques et hydrologiques réelles. Un scénario de crue a été pris en compte pour l'analyse des hauteurs d'eau et des vitesses d'écoulement dans le bassin. L'étude a mis en évidence l'intérêt de la modélisation hydraulique dans l'évaluation des risques d'inondation et a fourni des résultats utiles pour la planification territoriale et la prévention. Malgré certaines limites liées à la disponibilité des données et aux simplifications du modèle, ce travail souligne l'importance d'intégrer des outils scientifiques dans la gestion des aléas naturels.

Mots-clés : Risque d'inondation, Modélisation numérique, Simulation hydraulique, HEC-RAS, Bassin versant.

Table of Contents

List of Tables

List of Figures

List of Notations

Symbol / Abbreviation	Meaning / Description	Unit
Q	Flow rate (discharge)	m^3/s
Q_p	Peak flow rate	m^3/s
A	Area of watershed or cross-section	km^2 / m^2
h	Water depth / Height	m
g	Gravitational acceleration	9.81 m/s^2
t	Time	s / h
x	Longitudinal distance	m
L	River or channel length	m / km
T_p	Time to peak of hydrograph	h
T_c	Time of concentration	h
H_max, H_min	Maximum and minimum elevation	m
H_mean	Mean elevation of watershed	m
P	Precipitation	mm / cm
P_tc	Rainfall depth associated with time of concentration	mm
t_m, t_b	Rising time / Base time of hydrograph	h
Δt	Time step (numerical)	s
Δx	Spatial step (numerical)	m
R	Hydraulic radius	m
P_m	Wetted perimeter	m
S_0	Bed slope of river	dimensionless
S	General slope	% or ratio
n	Manning roughness coefficient	s/m^{1-3}
ρ	Water density	kg/m^3
u, v	Velocity components (x, y)	m/s
z	Bed elevation	m
a, F	Shape and form coefficients (e.g. Sokolovsky model)	-
θ	Angle (e.g. slope or direction)	degrees (°)
Dd	Drainage density	km/km^2
R_b	Bifurcation ratio	dimensionless
R_f	Form factor	dimensionless
DEM	Digital Elevation Model	-
CN	Curve Number (SCS method)	-
SCS	Soil Conservation Service	-
FDM	Finite Difference Method	-
FVM	Finite Volume Method	-
FEM	Finite Element Method	-
1D / 2D / 3D	Simulation dimensionality	-
HEC-RAS	Hydraulic modeling software	-
HEC-HMS	Hydrologic modeling software	-

GENERAL INTRODUCTION

General Introduction

Floods are recognized as one of the most frequent and destructive natural hazards worldwide, causing extensive damage to human life, infrastructure, ecosystems, and economic development (Kundzewicz et al., 2014). Their occurrence is governed by a complex interaction of climatic, topographical, hydrological, and anthropogenic factors. Notably, climate variability—such as changes in precipitation intensity and frequency—alongside alterations in land use, including deforestation and urban expansion, have significantly increased the vulnerability of many regions to flooding (IPCC, 2022). Moreover, the expansion of impermeable surfaces in urban areas disrupts natural hydrological processes, accelerating runoff and overwhelming drainage systems, thereby increasing the frequency and severity of flood events (Alfieri et al., 2015). As such, the development of accurate flood risk assessment tools and effective mitigation strategies has become a fundamental concern in environmental planning, civil engineering, and disaster management.

In response to these growing challenges, the present study adopts a numerical simulation approach using the HEC-RAS (Hydrologic Engineering Center – River Analysis System) software. Developed by the U.S. Army Corps of Engineers, HEC-RAS is a well-established tool for hydraulic modeling, capable of simulating both steady and unsteady flow regimes, computing water surface profiles, and delineating flood-prone areas (Brunner, 2020). The software integrates topographic and bathymetric data with hydrological inputs and geometric configurations, enabling the realistic modeling of complex river systems and flood scenarios. These capabilities are essential for understanding flood dynamics and supporting floodplain management and emergency planning (Horritt & Bates, 2002).

The application of HEC-RAS in this research aims to assess the hydrodynamic behavior of the Wadi El Hamiz watershed under various flood scenarios. By analyzing variables such as water depth, flow velocity, and flood extent, the study seeks to identify high-risk zones and provide technical support for the development of resilient, data-driven flood mitigation plans. As emphasized by Teng et al. (2017), coupling numerical simulations with geospatial and field data enhances the predictive capacity of flood models and strengthens disaster preparedness strategies.

Through the combination of scientific modeling tools and real-world data, this research contributes to the understanding of flood mechanisms in Mediterranean semi-urban environments. It also provides practical insights for local authorities and urban planners in

developing adaptive land-use strategies and reducing disaster vulnerability. Ultimately, the study seeks to bridge the gap between theoretical modeling and applied flood management practices.

This work is structured into four interconnected chapters, each contributing to the comprehensive assessment of hydraulic risk in the Wadi El Hamiz region.

Chapter 1 introduces the general concepts of flooding, including definitions, historical significance, classification of flood types, underlying causes, and their impacts on human societies and ecosystems.

Chapter 2 presents the principles of hydraulic modeling, focusing on the mathematical foundations (e.g., the Saint-Venant equations), numerical solution techniques, model dimensionality (1D/2D/3D), and a detailed overview of the HEC-RAS system.

Chapter 3 describes the study area—Wadi El Hamiz—by outlining its geographical, geological, climatic, and hydrological characteristics, with a particular focus on factors that contribute to its flood risk profile.

Chapter 4 applies the HEC-RAS model to simulate multiple flood scenarios, evaluate flood behavior, and map hydraulic risks to inform sustainable planning and effective risk mitigation strategies.

CHAPTER 1

1. General Concepts of Floods

1.1 Introduction

Floods are among the most widespread and recurrent natural phenomena, shaping landscapes and human societies since ancient times. Historically, civilizations such as those in Mesopotamia and the Indus Valley thrived alongside rivers, yet faced catastrophic consequences when floodwaters overtopped natural or human-made barriers. At their core, floods occur when water exceeds the capacity of a river, lake, or drainage system, inundating adjacent land. While often triggered by natural drivers like intense rainfall, snowmelt, or storm surges, human activities such as urbanization, deforestation, and poor land-use planning have increasingly exacerbated flood risks.

Floods are not uniform in their characteristics; they can be categorized into distinct types, such as river floods, coastal floods, or urban floods, etc. Each type poses unique challenges to communities, infrastructure, and ecosystems. Despite their natural origins, floods today are rarely purely “natural” disasters. Climate change, population growth, and encroachment into floodplains have intensified their frequency and severity, transforming them into complex socio-environmental crises.

The consequences of flooding are far-reaching, encompassing immediate human casualties, displacement, and infrastructure damage, as well as long-term disruptions to agriculture, economies, and public health. This chapter establishes the foundational concepts of floods, exploring their definitions, typologies, causes, and global significance, while underscoring the urgency of understanding these phenomena in an era of escalating climate extremes.

1.2 Definition of Floods

Floods are one of the most common and devastating natural disasters, resulting in significant loss of life and property damage worldwide. According to the World Meteorological Organization **(*WMO, 2012*)**, a flood is defined as *"the overflow of water onto normally dry land resulting from excessive rainfall, river overflow, or other hydrological conditions."* These events can occur when water bodies such as rivers, lakes, or seas rise above their usual levels and inundate surrounding areas. This overflow may be triggered by various factors, including heavy rainfall, rapid snowmelt, or a storm surge (***European Environment Agency, 2020***).

Floods can either be slow-onset or rapid-onset. Slow-onset floods, such as those caused by sustained heavy rainfall or snowmelt over time, build up gradually and may last for days or even weeks (IPCC, 2021). In contrast, flash floods occur suddenly, often within six hours of

intense rainfall, and typically cause widespread destruction over a short period (***Kundzewicz et al., 2014***).

1.3 History of Devastating Floods

Throughout human history, floods have been one of the most catastrophic natural disasters. Major flood events have shaped civilizations, economies, and political landscapes, often leading to widespread destruction, displacement, and loss of life. The history of devastating floods is marked by various occurrences, many of which remain deeply ingrained in historical records due to their immense scale and impact.

1.3.1 Ancient Civilizations and floods

Floods have been recorded as far back as ancient civilizations, where they were often seen as both natural occurrences and divine retribution. For example, the Mesopotamian civilization (modern-day Iraq) regularly experienced flooding due to the Tigris and Euphrates rivers. The Epic of Gilgamesh, one of the earliest works of literature, describes a catastrophic flood that wiped out humanity, reminiscent of the biblical flood story. Archaeological evidence suggests that floods frequently devastated ancient cities, leading to the collapse of early societies (***Barker, 2003***).

Similarly, ancient Egypt relied on the annual flooding of the Nile River, which was considered a blessing that provided fertile soil for agriculture. However, when these floods became too severe, they could cause widespread destruction, as was the case with the Nile flood of 1940, which resulted in the inundation of large agricultural lands and damage to the infrastructure of the region (**Kuper, 2016**).

1.3.2 The 20th Century: The Rise of Modern Flood Disasters

In the modern era, floods have been exacerbated by urbanization, climate change, and altered river systems. The 1931 China floods are often regarded as one of the deadliest flood events in recorded history. Triggered by prolonged rainfall and a series of typhoons, the Yangtze, Yellow, and Huai rivers all overflowed their banks, submerging vast areas in central and eastern China. It is estimated that between 1 million and 4 million people lost their lives due to drowning, disease, and famine (Chang, 2011). These floods also displaced millions of people and resulted in extensive economic damage.

In the United States, the Mississippi River flood of 1927 was another significant flood event, often cited as a turning point in flood management policy. The Mississippi River overflowed its banks following a period of heavy rainfall and snowmelt. This flood affected **seven states**,

with particularly severe damage in **Louisiana,** Arkansas, and Mississippi. Over 700,000 people were displaced, and the U.S. government responded by initiating large-scale flood control projects, including the construction of levees and dams, which would shape flood management strategies for decades to come (***Higgins, 2010***).

1.3.3 Recent Flood Disasters

In more recent years, devastating floods have continued to make headlines globally, exacerbated by human activities such as urbanization, deforestation, and climate change. One of the most significant flood events of the 21st century occurred in Pakistan in 2010. The 2010 Pakistan floods affected over 20 million people and caused widespread destruction across the country. The Indus River, which runs through Pakistan, experienced unprecedented flooding, driven by monsoon rains and glacial melt from the Himalayas. The floods destroyed homes, infrastructure, and agricultural lands, leaving millions without shelter and livelihood (***OCHA, 2010***).

The 2004 Indian Ocean Tsunami is another recent example of catastrophic flooding (***Fig 1.1***). While primarily caused by an underwater earthquake, the resulting tsunami generated massive floodwaters that devastated coastal regions in Indonesia, Sri Lanka, India, and Thailand. More than 230,000 people were killed, and the event highlighted the vulnerability of coastal communities to flooding and storm surges (***Løvholt et al., 2008***).

Fig 1.1. Impact of the 2004 Indian Ocean Tsunami in Banda Aceh, Indonesia (***National Oceanic and Atmospheric Administration, 2023***).

1.3.4 Factors Contributing to Modern Floods

Modern flood disasters are often compounded by human-induced factors such as urbanization and environmental degradation. Cities, particularly those with inadequate drainage systems, are increasingly vulnerable to pluvial floods (surface water flooding). For example, the 2010 floods in Pakistan were exacerbated by the construction of dams and the destruction of wetlands, which reduced the land's natural ability to absorb water (***OCHA, 2010***). Similarly, the 2015 floods in Myanmar were largely caused by both excessive rainfall and deforestation in the surrounding mountainous regions, which led to massive soil erosion and river overflow (***Brammer, 2016***).

The impact of climate change is also becoming more evident in flood events. Rising global temperatures contribute to more intense and frequent rainfall, as well as rising sea levels, which increase the risk of coastal flooding (***IPCC, 2021***). A recent example of this is Hurricane Katrina in 2005, which led to catastrophic flooding in New Orleans, Louisiana, and is often cited as a stark example of how urbanization, inadequate infrastructure, and climate change contribute to flood disasters (***Baker, 2006***).

1.4 Hydrological Characteristics of Floods

The characteristics of floods are determined by a range of hydrological parameters. These include:

- **Peak Discharge**: The maximum flow rate of water during a flood event, often measured in cubic meters per second (***WMO, 2012***).
- **Flood Duration**: The length of time over which the floodwaters persist (***IPCC, 2021***).
- **Flood Extent**: The geographical area that becomes submerged during the flood event, which can be predicted using flood mapping techniques (***Global Water Partnership, 2004***).

Understanding these characteristics is essential for flood risk management, as they help define flood frequency, predict flood behavior, and develop mitigation strategies (***European Environment Agency, 2020***).

1.5 Types of Floods

Floods can be categorized in various ways based on their origin, behavior, and the rate at which they occur. These distinctions are important for understanding the underlying causes of floods and developing appropriate flood management strategies. The types of floods can generally be

classified into river floods, coastal floods, urban floods, flash floods, and pluvial floods, among others. Each type has distinct characteristics and requires different strategies for mitigation and management.

1.5.1 River (Fluvial) Floods

River floods, also known as fluvial floods, are caused by the overflow of rivers due to heavy rainfall or snowmelt, which increase the volume of water flowing through the river channels. When the river's discharge exceeds its capacity, it overflows onto adjacent floodplains, submerging surrounding areas (***Fig 1.2***). These types of floods can be slow to develop, often taking days or weeks to reach their peak. The Mississippi River Flood of 1927 is one of the most well-known examples of this type of flood. This event occurred after a period of heavy rainfall and snowmelt, causing the Mississippi River to overflow its banks and flood large parts of the American South, displacing hundreds of thousands of people (***Higgins, 2010***).

River floods are typically seasonal, with the risk of flooding being highest during the rainy season or spring melt. However, they can also occur due to dam failures, as seen with the Banqiao Dam disaster in China (1975), where the collapse of a dam led to catastrophic flooding in nearby regions (Wang, 2015).

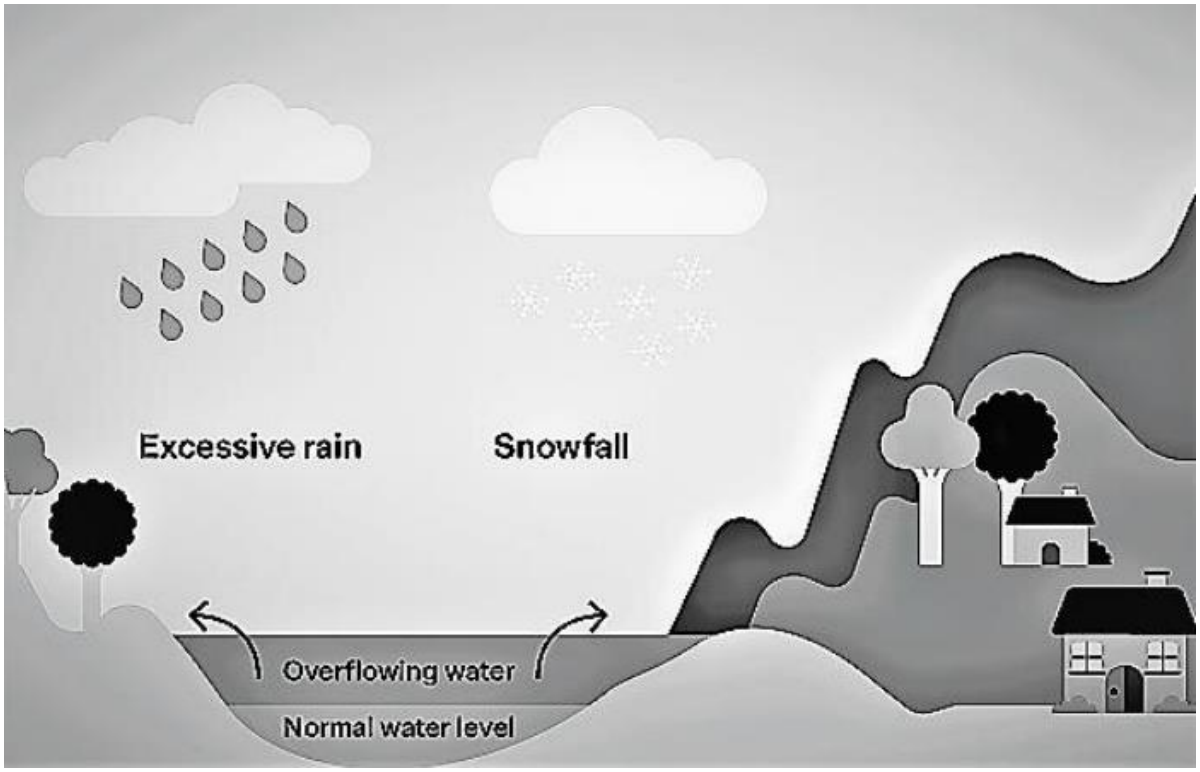

Fig 1.2. River floods type (***Mardaid et al., 2023***).

1.5.2 Coastal Floods

Coastal floods occur when high tides, storm surges, or tsunamis cause seawater to inundate coastal regions. These types of floods are particularly dangerous in areas where large populations live near the coast. Coastal floods can be triggered by extreme weather events such as hurricanes, cyclones, or typhoons, which generate storm surges that push seawater inland (***Fig 1.3***). For example, Hurricane Katrina in 2005 led to widespread flooding in New Orleans, Louisiana, after the storm surge overwhelmed levees, causing water to inundate the city (***Baker, 2006***). Similarly, the 2004 Indian Ocean tsunami, triggered by an undersea earthquake, generated massive waves that flooded coastal areas of several countries, including Indonesia, Sri Lanka, and Thailand, leading to catastrophic loss of life and property (***Løvholt et al., 2008***).

Coastal flooding is a growing concern due to rising sea levels linked to climate change, which exacerbates the risk of storm surges and tidal flooding (***IPCC, 2021***).

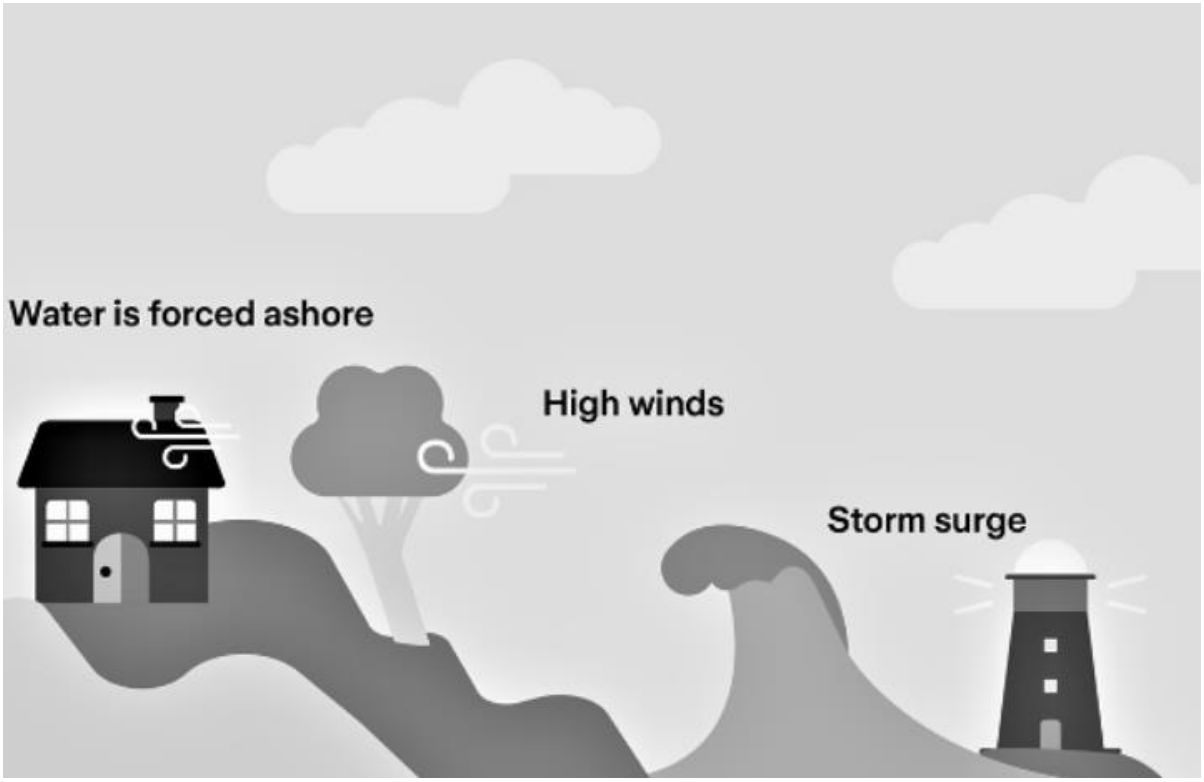

Fig 1.3. Coastal floods type (***Mardaid et al., 2023***).

1.5.3 Urban Floods

Urban floods occur in cities and towns when the local drainage systems are overwhelmed by heavy rainfall, leading to water accumulation on streets and in buildings (***Fig 1.4***). These floods are often exacerbated by the high concentration of impermeable surfaces such as concrete, asphalt, and buildings, which prevent water from being absorbed into the ground. Additionally,

poorly designed or outdated drainage systems can lead to water backing up into streets, resulting in localized flooding.

The 2010 floods in Mumbai, India, are a notable example of urban flooding. These floods were caused by extremely heavy monsoon rains that overwhelmed the city's drainage system, leading to widespread damage to infrastructure and property (***Brammer, 2016***). Urban floods are particularly dangerous due to their rapid onset, limited time for response, and the large number of people affected in densely populated areas.

Fig 1.4. Urban floods in Golestan province (***Zhang et al., 2021***).

1.5.4 Flash Floods

Flash floods are fast-moving floods that occur with little warning, typically within six hours of intense rainfall or other triggering events such as a dam break (***Fig 1.5***). Flash floods can be particularly deadly due to their rapid onset and the difficulty in predicting their occurrence. These floods are common in areas with steep terrain or in urban environments where water runoff is concentrated into narrow channels.

The 2005 flooding in London is an example of flash flooding caused by intense rainfall. This event resulted in significant damage to transportation systems and caused the displacement of

thousands of residents (***Hughes, 2006***). Flash floods are also often linked to landslides and debris flows, which can further complicate rescue efforts (***Baker, 2006***).

Fig 1.5. Flash floods in in the valley of the Sanna River in Modliborzyce municipality (***Baran-Zgłobicka et al., 2021***).

1.5.5 Pluvial (Surface Water) Floods

Pluvial floods occur when heavy rainfall accumulates on the ground faster than it can be absorbed or drained away, leading to surface water flooding. Unlike river floods, which are related to the overflow of rivers, pluvial floods are the result of localized rainfall that overwhelms the capacity of urban drainage systems or the natural drainage of an area. These floods are most common in urbanized areas with high impervious surfaces (***Fig 1.6***).

The 2016 flash floods in Paris were a classic example of pluvial flooding, where sudden and heavy rainfall overwhelmed the city's drainage infrastructure, flooding streets and causing transportation disruptions (***Hughes, 2006***). Similarly, the 2005 Mumbai floods were a combination of urban flooding and pluvial flooding, exacerbated by inadequate drainage and the city's rapid urban expansion (***Brammer, 2016***).

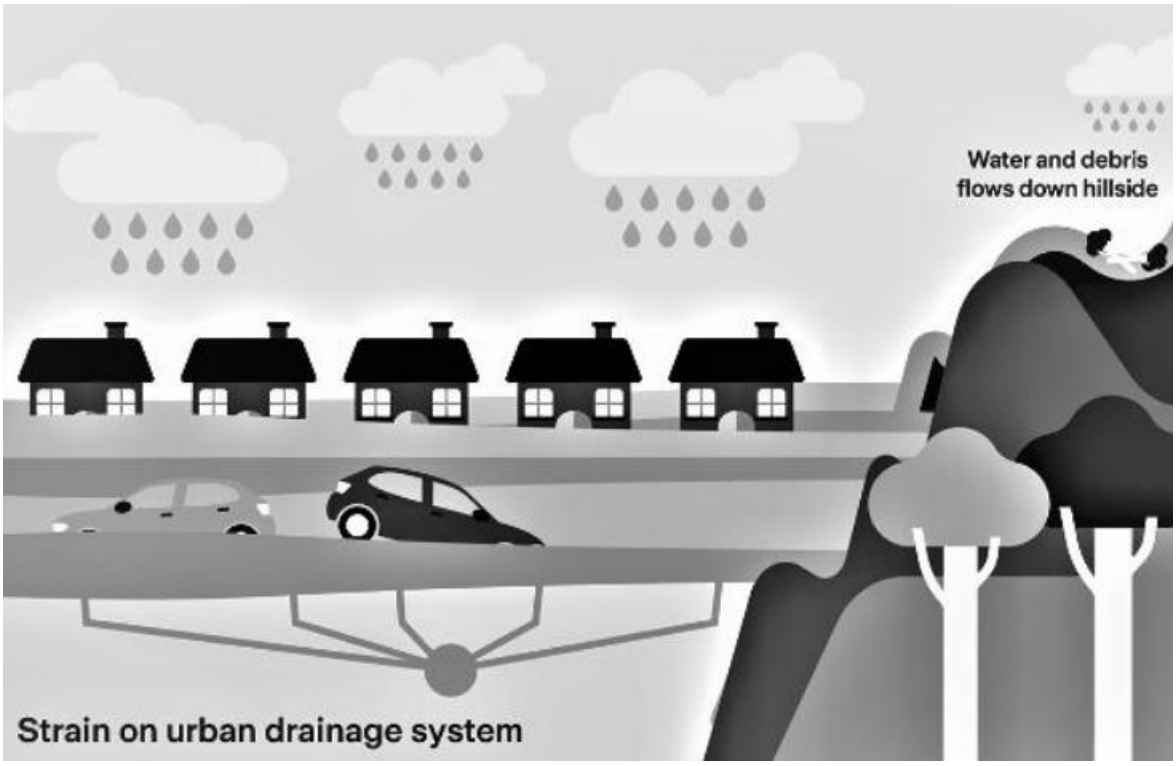

Fig 1.6. Pluvial floods type (***Mardaid et al., 2023***).

1.6 Causes of Floods

Floods result from a combination of natural and human-induced factors. Natural causes include heavy and prolonged rainfall, rapid snowmelt, and storm surges due to atmospheric conditions such as hurricanes (**Kundzewicz et al., 2014**). On the other hand, human-induced causes often involve urbanization, deforestation, and poor land use management, which increase flood vulnerability (***Global Water Partnership, 2004***).

For example, urbanization is a major contributing factor to pluvial floods in cities. The expansion of concrete surfaces reduces the ability of soil to absorb water, causing an increase in surface runoff and overwhelming stormwater drainage systems (***UNDRR, 2019***). Deforestation further exacerbates flooding as trees play a crucial role in absorbing water and preventing soil erosion (***IPCC, 2021***). Climate change also contributes to more extreme weather events, increasing the frequency and severity of floods (***IPCC, 2021***).

Table 1.1: Causes of Floods Classified by Natural and Human-Induced Factors.

Natural Causes	Human Causes
Heavy rainfall	Urbanization (impervious surfaces)
Snowmelt	Deforestation
Storm surges	Poor land management
Tsunamis	Climate change

Floods are the result of a complex interaction between natural and human-induced factors. The primary causes of floods include excessive rainfall, snowmelt, dam failures, storm surges, and poor land management practices. These causes can either be natural or exacerbated by human activities, particularly in urbanized and deforested areas.

1.6.1 Excessive Rainfall

One of the most common causes of flooding is excessive rainfall, which can overwhelm the natural drainage systems and the capacity of rivers and streams. When the amount of rainfall exceeds the ground's ability to absorb it or the flow capacity of rivers, floodwaters are generated. This is often seen in riverine (fluvial) floods and pluvial (surface water) floods.

In urban areas, the rapid buildup of rainfall often leads to surface water flooding because impermeable surfaces like roads, buildings, and pavements prevent the natural absorption of water into the ground. This is a major cause of flash floods, especially in cities that lack adequate drainage systems (***UNDRR, 2019***). The 2010 Pakistan floods, for example, were driven by an intense monsoon season that caused river and surface water flooding, displacing millions of people (***OCHA, 2010***).

1.6.2 Snowmelt

In colder climates, the rapid melting of snow in the spring can contribute to river floods. Snowmelt is a significant contributor to the seasonal rise in river discharge, especially in mountainous regions or areas near glaciers. When large amounts of snow melt at once due to rising temperatures or sudden warmth, rivers can experience a sudden increase in volume, leading to overflow.

For instance, in North America, the Missouri River floods are often triggered by a combination of spring snowmelt and heavy rainfall. In China, snowmelt from the Himalayas and other mountain ranges contributes significantly to river floods, as seen in the 2010 Yellow River floods (***IPCC, 2021***).

1.6.3 Dam Failures

Dam failures are another significant cause of floods. When dams or levees that are designed to control water flow fail due to structural issues, mismanagement, or natural disasters such as earthquakes or heavy rainfall, the resulting floodwaters can inundate large areas. Dam failure floods are typically catastrophic due to the large volumes of water involved.

The Banqiao Dam disaster in China in 1975 is one of the deadliest instances of dam failure. After a period of intense rainfall, the dam's structural integrity was compromised, leading to the

release of massive floodwaters that killed over 170,000 people and displaced millions (***Wang, 2015***). Similarly, the 2019 Kerala floods in India were partly caused by the release of water from multiple reservoirs in the region, which had been forced to open their gates to prevent dam breaches due to excessive rainfall (***Brammer, 2016***).

1.6.4 Storm Surges

Storm surges are another major cause of flooding, particularly in coastal areas. These occur when strong winds from tropical storms or hurricanes push seawater onto the land, resulting in coastal flooding. Storm surges are often accompanied by heavy rainfall and can cause widespread destruction in coastal communities.

The 2004 Indian Ocean Tsunami, triggered by an undersea earthquake, led to massive storm surges that devastated coastal areas in Indonesia, Sri Lanka, India, and Thailand (***Løvholt et al., 2008***). Similarly, Hurricane Katrina in 2005 caused catastrophic storm surge flooding in New Orleans, Louisiana, after the storm's powerful winds pushed water into the city's vulnerable low-lying areas (***Baker, 2006***).

1.6.5 Deforestation and Poor Land Use Management

Human activities, especially deforestation and poor land management practices, have significantly exacerbated the risk of flooding. Forests play a crucial role in absorbing water and regulating river flows. When large areas of forest are cleared for agriculture, urban development, or logging, the ability of the land to absorb water is significantly reduced. This results in increased surface runoff, which can overwhelm rivers and drainage systems.

In addition, the construction of buildings and roads in flood-prone areas, particularly in floodplains and wetlands, increases the risk of urban floods. The 2010 Pakistan floods were partly caused by the combination of deforestation, rapid urbanization, and poor land management, which contributed to the severity of the event (***OCHA, 2010***).

Soil erosion, another result of poor land use practices, can also increase flood risk. Without the stabilizing influence of vegetation, soil is more likely to be washed away by heavy rainfall, further increasing runoff and contributing to river and surface water flooding (***IPCC, 2021***).

1.6.6 Climate Change

One of the most pressing contemporary causes of flooding is climate change, which is altering weather patterns and increasing the frequency and intensity of extreme weather events. Rising global temperatures are leading to more intense rainfall events, rapid snowmelt, and rising sea

levels, all of which contribute to an increased risk of flooding. Coastal communities are particularly vulnerable to storm surge and tidal flooding due to rising sea levels.

Hurricane Katrina, one of the deadliest storms in U.S. history, was exacerbated by the effects of climate change, which led to higher-than-normal sea surface temperatures and more powerful storm surges (***Baker, 2006***). Similarly, the 2017 Hurricane Harvey was characterized by extreme rainfall, which overwhelmed the flood protection systems of Houston, Texas, leading to widespread flooding (***IPCC, 2021***).

1.7 Impacts of Floods

Floods are one of the most devastating natural disasters, affecting both the environment and human societies in a multitude of ways. The impacts of floods can be economic, social, environmental, and public health-related. These impacts often extend far beyond the immediate aftermath, as the long-term consequences of floods can persist for years, particularly in areas that are frequently inundated. Understanding these impacts is crucial for effective flood management and prevention.

1.7.1 Economic Impacts

The economic impacts of floods are often the most immediately visible and quantifiable. The damage to infrastructure, businesses, and homes can lead to significant financial losses. Flooding can disrupt local economies by destroying crops, manufacturing facilities, roads, bridges, and power lines, thus impairing supply chains and access to essential services. Insurance claims rise substantially, and governments often face enormous costs in the aftermath of floods, from emergency relief operations to long-term recovery and rebuilding.

For instance, the 2011 Thailand floods had a devastating economic impact on the country, with losses estimated at $45 billion. The floods submerged large parts of the country's industrial zones, affecting major global manufacturing companies, particularly in the automotive and electronics industries (***Hossain, 2013***). Similarly, Hurricane Katrina in the United States in 2005 caused widespread damage to infrastructure, resulting in an estimated $125 billion in economic losses, including the costs of rebuilding homes, roads, and public services (***Baker, 2006***).

Floods can also affect the agriculture sector, leading to crop failure, livestock deaths, and the destruction of farmland. This can lead to food shortages and price increases, further exacerbating the economic strain. The 2010 Pakistan floods devastated agricultural regions, resulting in an estimated $2.9 billion in crop and livestock losses (***OCHA, 2010***).

1.7.2 Social Impacts

The social impacts of floods are profound, affecting communities, displacing populations, and disrupting social structures. Flooding often leads to the displacement of thousands of people, forcing them to leave their homes and seek shelter in temporary camps or evacuation centers. This can lead to the breakdown of social networks and create long-term challenges for resettlement and community rebuilding.

In many cases, the disruption of daily life can lead to a decline in mental health. The trauma associated with losing homes, loved ones, and livelihoods can lead to depression, anxiety, and post-traumatic stress disorder (PTSD) in affected individuals. The 2010 Pakistan floods displaced over 20 million people, leaving them without homes, food, and access to healthcare, and contributing to significant psychological distress (***OCHA, 2010***).

Floods can also exacerbate existing social inequalities. Vulnerable populations, such as the poor, elderly, and disabled, are often the hardest hit. These groups may lack the resources to evacuate or rebuild, leading to longer recovery times and greater hardships. Women and children are particularly vulnerable in the aftermath of floods, as they may face greater exposure to gender-based violence and exploitation in emergency settings (***UNICEF, 2015***).

1.7.3 Environmental Impacts

Floods can have severe environmental impacts, especially when they occur in areas with sensitive ecosystems. The inundation of land and the destruction of vegetation can lead to soil erosion, water pollution, and the destruction of habitats. In agricultural areas, the floodwaters often carry pollutants, chemicals, and waste from industrial zones, which can degrade water quality and harm aquatic ecosystems.

For example, the 2011 Thailand floods caused significant damage to the Chao Phraya River, with floodwaters washing large amounts of debris, waste, and chemical pollutants into the water. This not only damaged local biodiversity but also caused long-term ecological damage to the river's health (***Hossain, 2013).***

Floods can also result in wetland loss, which can further exacerbate flooding in the future. Wetlands play a crucial role in regulating water flow, filtering water, and providing habitat for wildlife. When they are damaged or destroyed by flooding, the natural system that helps mitigate floods becomes less effective. This can lead to a cycle of increasing flood severity over time, particularly in flood-prone areas.

1.7.4 Public Health Impacts

Floods have significant public health consequences, both during and after the event. The immediate aftermath of a flood often involves waterborne diseases, which can spread rapidly in flood-affected areas. Cholera, typhoid, dysentery, and hepatitis A are common diseases that thrive in flooded environments due to contaminated drinking water and poor sanitation facilities. The lack of clean water and proper hygiene facilities further exacerbates the spread of these diseases.

In addition to infectious diseases, floods can also increase the risk of vector-borne diseases such as malaria and dengue fever. Standing water in flooded areas creates ideal breeding grounds for mosquitoes, which can spread diseases in the affected population. For instance, the 2015 Chennai floods in India led to an increase in dengue and malaria cases as stagnant water allowed mosquitoes to breed in large numbers (***WHO, 2016***).

The mental health impact is also significant. Flood survivors often experience high levels of stress, trauma, and mental health disorders due to loss of property, loved ones, and livelihoods. Efforts to provide psychological support and mental health services are critical in the aftermath of floods to mitigate these effects (***UNICEF, 2015***).

1.7.5 Long-Term Effects

The long-term effects of floods are often overlooked but can be as devastating as the immediate impacts. The disruption of daily life, loss of livelihoods, and damage to infrastructure can leave communities struggling to recover for years. In some cases, entire regions may face a long-term decline in quality of life as they work to rebuild and restore services.

Floods can also have a political impact, as the mismanagement of flood responses or recovery efforts can lead to public dissatisfaction, protests, and even changes in government leadership. The response to Hurricane Katrina in the United States, for instance, highlighted issues related to governmental preparedness and response, leading to significant political fallout (***Baker, 2006***).

1.8 Conclusion

Floods are one of the most destructive natural disasters, with significant effects on people, economies, the environment, and public health. Their impacts are not limited to the immediate destruction but also extend over the long term, affecting recovery and resilience. The economic consequences of floods can be overwhelming, as they damage infrastructure, homes, businesses, and agriculture, often causing long-term financial strain.

Socially, floods disrupt communities and displace large numbers of people. Vulnerable populations, such as the elderly, children, and those in poverty, suffer the most from the consequences of flooding. Mental health issues, including stress and trauma, are common among survivors, adding another layer of difficulty to recovery.

Environmentally, floods lead to the destruction of natural habitats, soil erosion, and water contamination. These environmental impacts can have lasting effects on biodiversity and exacerbate future flood risks. Additionally, floods often contribute to the spread of waterborne diseases, which pose a serious health threat, especially in areas with damaged infrastructure and inadequate sanitation.

In conclusion, understanding the causes and impacts of floods is crucial for improving flood management strategies. Effective prevention, preparedness, and recovery efforts are necessary to minimize the damage and help communities recover more quickly. By addressing the root causes of floods and implementing comprehensive flood management practices, we can reduce the long-term impacts of floods and build more resilient societies.

CHAPTER 2

2 Hydraulic Flood Modeling

2.1 Introduction

Floods are among the most devastating natural hazards worldwide. They are responsible for significant loss of life, property damage, and long-term socio-economic impacts (**Kundzewicz et al., 2014**). Understanding the dynamics of floods has become increasingly important, particularly in the context of climate change and rapid urban expansion.

Hydraulic modeling serves as a key tool for simulating the behavior of water flows during such events, enabling the identification of risk zones and supporting effective flood risk management strategies (**Horritt & Bates, 2002**).

2.1. Definition of Hydraulic Modeling

Hydraulic modeling refers to the mathematical simulation of water movement through natural or engineered channels, floodplains, and drainage networks. It is generally based on the Saint-Venant equations — a set of partial differential equations describing the conservation of mass and momentum in open channel flows (**Chow et al., 1988**).

- 1D Modeling: Simulates flow along a primary direction (typically along a river channel), assuming uniform flow distribution across cross-sections.
- 2D Modeling: Simulates flows in both horizontal directions, capturing more detailed interactions, particularly useful in urban or floodplain environments.

2.2 Objectives of Hydraulic Modeling

Hydraulic flood modeling is used for several key purposes:

- Identifying flood-prone areas under various scenarios.
- Estimating water surface elevations, flow depths, and velocities.
- Simulating extreme events, infrastructure failure (e.g., levee breach), or land-use changes.
- Supporting risk-informed decision-making in flood management and urban planning (**de Moel & Aerts, 2009**).

2.3 Mathematical Modeling

Mathematical modeling is the foundation of hydraulic simulation, providing a systematic approach to describing the physical behavior of fluid flows, especially in rivers, channels, and floodplains. By translating the principles of fluid mechanics into solvable mathematical

equations, engineers and scientists can simulate the spatial and temporal evolution of floods. Among the most important equations used in hydraulic modeling are the Saint-Venant equations, which describe unsteady open-channel flow (**Chow et al., 1988; Cunge et al., 1980**).

2.3.1 The Saint-Venant Equations

The Saint-Venant equations are a set of partial differential equations derived from the fundamental principles of mass conservation (continuity) and momentum conservation. They are used to describe the movement of shallow water in rivers, channels, and overland surfaces under free-surface conditions, where the pressure distribution is hydrostatic.

These equations were first formulated by Adhémar Jean Claude Barré de Saint-Venant in 1871 and remain the cornerstone of hydraulic flow modeling today (**Saint-Venant, 1871**).

2.3.1.1 Assumptions of the Saint-Venant Equations

To simplify the complex three-dimensional Navier-Stokes equations into a more manageable form for open-channel flows, the following assumptions are made:

- The fluid is incompressible.
- The pressure distribution is hydrostatic (valid for shallow flows).
- Vertical accelerations are negligible.
- The flow is one- or two-dimensional.
- Channel bed slope is small.

These assumptions are generally valid for rivers, canals, and floodplains under natural conditions (**Fread, 1993**).

2.3.1.2 One-Dimensional Saint-Venant Equations

In 1D form, the Saint-Venant equations consist of:

Continuity Equation (Conservation of Mass):

$$\frac{\partial \mathrm{A}}{\partial \mathrm{t}} + \frac{\partial \mathrm{Q}}{\partial \mathrm{x}} = q_L \tag{2.1}$$

- Where :
- A: Cross-sectional area (m^2).
- Q: Discharge (m^3/s).
- x: Longitudinal distance (m).
- t : Time (s).
- q_L: Lateral inflow per unit length (m^2/s).

Momentum Equation (Conservation of Momentum):

$$\frac{\partial Q}{\partial t} + \frac{\partial}{\partial x}\left(\frac{Q^2}{A}\right) + gA\frac{\partial h}{\partial x} = gA(S_0 + S_f) + q_L v_L \quad (2.2)$$

Where :

- h: Water depth (m).
- g: Acceleration due to gravity (9.81 m/s²).
- S_0: Channel bed slope.
- S_f: Friction slope.
- v_L: Velocity of lateral inflow (m/s).

These equations describe how discharge and water surface elevation change over time and space.

2.3.1.3 Two-Dimensional Saint-Venant Equations

In cases where flow direction cannot be assumed to be unidirectional — such as in wide floodplains, urban areas, or after levee breaches — the 2D form of the Saint-Venant equations is preferred. These are written in terms of water depth h, and the unit discharges (q_x=hv) and (q_y= hv) where u and v are the depth-averaged velocity components in the x and y directions respectively.

Continuity Equation (2D):

$$\frac{\partial h}{\partial t} + \frac{\partial (hu)}{\partial x} + \frac{\partial (hv)}{\partial y} = r \quad (2.3)$$

Momentum Equations (x and y directions):

$$\frac{\partial (hu) + \frac{\partial (hu^2 + \frac{1}{2}gh^2)}{\partial x} + \frac{\partial (huv)}{\partial y} = -gh\frac{\partial z}{\partial x} - T_{bx}/P}{\partial t}$$
$$\frac{\partial (hv)}{\partial t} + \frac{\partial (huv)}{\partial x} + \frac{\partial (hv^2 + \frac{1}{2}gh^2)}{\partial y} = -gh\frac{\partial z}{\partial x} - T_{by}/P \quad (2.4)$$

- Where :

- z: Bottom elevation.
- T_{by}, T_{bx} : Bottom shear stresses.
- P: Water density.

These equations are more computationally intensive but offer greater accuracy in simulating flow patterns in complex geometries (**Zoppou & Roberts, 2000**).

2.3.2 Numerical Solution Methods

Hydraulic modeling of floods involves solving complex systems of partial differential equations, notably the Saint-Venant equations. These equations, while fundamental in describing unsteady open-channel flow, are nonlinear and do not have general analytical solutions, they are solved using numerical methods. The choice of method influences the accuracy and stability of the simulation.

- Finite Difference Method (FDM): Approximates derivatives using differences between grid points. Used in early flood models but less stable for complex flows.
- Finite Volume Method (FVM): Integrates the equations over discrete volumes, conserving mass and momentum explicitly.
- Finite Element Method (FEM): Ideal for complex geometries but computationally expensive.

Modern software such as HEC-RAS, MIKE FLOOD, and Iber implement robust numerical schemes like Godunov-type solvers, implicit-explicit schemes, and adaptive time stepping to solve these equations efficiently (**Brunner, 2020**).

2.3.2.1 Boundary and Initial Conditions

Accurate definition of boundary and initial conditions is critical for realistic simulations:

- Upstream boundaries typically involve inflow hydrographs.
- Downstream boundaries can be defined using rating curves or water surface elevations.
- Initial conditions include starting water levels and flow velocities.

Poorly defined boundaries can lead to instabilities or incorrect predictions, particularly in unsteady simulations (**Pappenberger et al., 2005**).

2.3.2.2 Limitations and Uncertainties

While the Saint-Venant equations provide a reliable basis for hydraulic modeling, several limitations must be acknowledged:

- Assumes hydrostatic pressure (not valid in rapidly varied or vertical flows).
- Sensitive to input data (e.g., topography, Manning's n).
- Requires calibration and validation against observed data.
- Computational demand increases in 2D or fine-resolution models.

These challenges can be mitigated through sensitivity analysis, model validation, and the use of high-quality input data (**Beven, 2011**).

2.3.2.3 General Principles of Numerical Resolution

Numerical methods aim to convert the continuous spatial and temporal domain of the equations into a discrete computational grid, where approximate solutions can be calculated step-by-step. The essential steps are:

1. Spatial Discretization: Dividing the river or floodplain into nodes or cells.
2. Temporal Discretization: Solving the equations over successive time steps.
3. Stability Considerations: Ensuring that the method remains stable over time (e.g., respecting the Courant-Friedrichs-Lewy (CFL) condition).
4. Boundary Conditions: Applying known values at the domain edges.

The choice of method directly impacts the accuracy, stability, and efficiency of the simulation (**Fletcher, 1991**).

2.3.2.4 Finite Difference Method (FDM)

The finite difference method approximates derivatives by differences between grid points. It is one of the oldest and most straightforward techniques for solving the Saint-Venant equations.

Example:

$$\frac{\partial h}{\partial t} \approx \frac{h_i^{n+1} - h_i^n}{\Delta t} \tag{2.5}$$

- Advantages: Easy to implement; computationally efficient.
- Disadvantages: Less accurate near boundaries or in complex geometries; can become unstable without careful time-step selection.

FDM is commonly used in structured grid environments and 1D river models like HEC-RAS (implicit scheme) (**Brunner, 2020**).

2.3.2.5 Finite Volume Method (FVM)

The finite volume method integrates the governing equations over discrete control volumes. It is conservative by design, ensuring that mass and momentum are preserved across cells — an important feature for flood modeling.

- Advantages:
    - Handles shock waves and discontinuities well.
    - Applicable in both structured and unstructured grids.
    - Ideal for 2D modeling.
- Common Schemes:
    - Godunov-type schemes (e.g., HLL, Roe)
    - MUSCL (Monotonic Upstream-centered Schemes for Conservation Laws) for higher-order accuracy

FVM is the core method used in modern 2D solvers such as Iber, MIKE 21, and HEC-RAS 2D (**Zoppou & Roberts, 2000**).

2.3.2.6 Finite Element Method (FEM)

The finite element method subdivides the domain into smaller elements and applies interpolation functions to approximate the solution.

- Advantages:
    - Highly flexible in modeling irregular boundaries and geometries.
    - Strong theoretical foundation for convergence and error estimation.
- Disadvantages:
    - Computationally intensive.
    - Complex to implement compared to FDM and FVM.

FEM is commonly used in hydrodynamic solvers with high geometric complexity **(Huyakorn & Pinder, 1983**).

2.3.2.7 Explicit vs. Implicit Schemes

- **Explicit Schemes**:
    - Calculate the solution at the next time step directly from known values.
    - Simpler and faster per time step, but conditionally stable (requires small Δt for stability).
- **Implicit Schemes**:
    - Involve solving a system of equations at each time step.
    - More stable, allowing larger time steps, but computationally more expensive per step.

Most software, including HEC-RAS, uses semi-implicit or fully implicit schemes for unsteady flow modeling (**Fread, 1993**).

2.3.2.8 Stability and Accuracy

A major consideration in numerical modeling is balancing stability and accuracy:

- Stability: Ensured by respecting the CFL condition:

$$CFL = \frac{u\Delta t}{\Delta x} \leq 1 \tag{2.6}$$

- Accuracy: Affected by spatial and temporal resolution, interpolation schemes, and numerical diffusion.

Model calibration and grid refinement studies are often necessary to optimize both (**Pappenberger et al., 2005**).

2.3.3 Implementation in Software

Modern hydraulic modeling software integrates numerical solvers with GIS tools, enabling user-friendly interfaces and real-time visualization. Examples include:

- HEC-RAS: Combines FDM (1D) and FVM (2D); uses semi-implicit schemes.
- Iber: Open-source 2D solver based on FVM and GPU acceleration.
- MIKE FLOOD: Commercial software supporting coupled 1D/2D modeling with advanced numerical engines.
- TELEMAC-2D: Finite element-based, highly accurate for coastal and riverine simulations.

These tools implement robust pre- and post-processing, automated mesh generation, and flexible boundary condition settings.

2.4 Different Types of Hydraulic Modeling – 1D, 2D, and 3D Simulation

Hydraulic modeling can be approached through various levels of spatial and temporal complexity depending on the objectives of the study, available data, and computational resources. The most common classification is based on the number of spatial dimensions represented in the model: 1D (one-dimensional), 2D (two-dimensional), and 3D (three-dimensional). Each modeling type has unique capabilities, assumptions, advantages, and limitations.

This chapter presents a comparative analysis of the different types of simulation used in flood modeling, emphasizing their structure, applications, and integration in modern software platforms.

2.4.1 One-Dimensional (1D) Modeling

In 1D modeling, the flow is assumed to occur **predominantly in one direction** — usually along the main channel of a river. Cross-sectional variations in velocity and water depth are neglected or parameterized. The **Saint-Venant equations in 1D form** are used to describe the flow (as discussed in Chapter 2).

Applications

- River and channel routing
- Flood wave propagation
- Dam-break studies along narrow valleys
- Sewer or pipe network modeling

Advantages

- Fast computation
- Simple setup

Limitations

- Cannot capture lateral flow or detailed floodplain dynamics
- Poor accuracy in urban or highly branched systems

- Cannot simulate flow splitting or recirculation

Tools

HEC-RAS 1D, MIKE 11, SOBEK

Brunner (2020) highlights that HEC-RAS 1D remains a benchmark tool for regulatory floodplain delineation when lateral variability is limited.

2.4.2 Two-Dimensional (2D) Modeling

2D models solve the depth-averaged Saint-Venant equations in both horizontal directions (x and y). They simulate variations in water depth and velocity across a surface, making them ideal for floodplain dynamics, urban flooding, and coastal inundation.

Applications

- Overbank flooding and flood mapping
- Urban drainage with surface flow
- Levee breach and dam break analysis
- Tsunami and storm surge modeling

Advantages

- Realistic representation of flow patterns
- Can simulate flow around buildings, roads, terrain features
- Supports spatially distributed rainfall and infiltration

Limitations

- Requires detailed topography (DEM)
- More computationally intensive
- Needs careful mesh generation and calibration

Tools

HEC-RAS 2D, Iber, MIKE 21, TELEMAC-2D

Zoppou and Roberts (2000) demonstrated the advantages of 2D modeling in simulating complex flood propagation after dam failures.

2.4.3 Three-Dimensional (3D) Modeling

3D models solve the full Navier-Stokes equations, accounting for velocity components in all three directions (x, y, and z). This allows simulation of vertical flow structures, turbulence, and stratification, which cannot be captured in 1D or 2D.

Applications

- Flow around structures (bridges, piers, dams)
- Sediment transport and scour analysis
- Hydraulic jumps and vortices
- Estuary, reservoir, or coastal circulation

Advantages

- Highly detailed results
- Captures vertical flow and 3D turbulence
- Required for advanced sediment and pollutant transport studies

Limitations

- Extremely demanding in terms of data, calibration, and computation
- Rarely used for large-scale floodplain simulation
- Requires high-level expertise

Tools

FLOW-3D, OpenFOAM, Delft3D-FLOW, ANSYS Fluent

Huyakorn et al. (1987) emphasize that 3D models are essential when vertical mixing and flow complexity cannot be neglected, such as in reservoir circulation studies.

The following table summarize the different modeling types.

Table 2.1: Modeling types characteristics

Feature	1D	2D	3D
Flow Direction	Longitudinal	Longitudinal + Lateral	Fully 3D (x, y, z)
Governing Equations	1D Saint-Venant	2D Saint-Venant	Navier-Stokes
Computational Cost	Low	Moderate	High
Input Data	Cross-sections	DEM, land use	Full bathymetry + turbulence data
Applications	Rivers, canals	Floodplains, urban flooding	Scour, reservoir, detailed flow
Accuracy	Moderate	High (for surface flows)	Very high (in complex flows)

2.5 Choosing the Appropriate Model

The selection of a modeling approach depends on several factors:

- Objective of the study: Mapping flood extents (2D), simulating bridge scour (3D), flood routing (1D).
- Availability of data: DEMs for 2D; bathymetry and flow data for 3D.
- Computation time: Limited resources may favor 1D or hybrid 1D/2D models.
- Domain complexity: Urban areas typically require at least 2D simulation.

In many real-world projects, hybrid models are used — for example, combining 1D river routing with 2D floodplain mapping in HEC-RAS or MIKE FLOOD.

2.6 Modeling Commercial Tools

Several tools have been developed for hydraulic modeling. Among the most widely used:

Hydraulic Flood Modeling

- **HEC-RAS** (Hydrologic Engineering Center's River Analysis System), developed by the U.S. Army Corps of Engineers. It allows for the simulation of steady and unsteady flow regimes in both 1D and 2D modes (**Brunner, 2020**).
- **MIKE FLOOD**, developed by DHI, integrates hydrological and hydraulic modeling.
- **Iber**, an open-source 2D hydrodynamic modeling tool based on the Saint-Venant equations.

2.7 Limitations and Uncertainties

Despite its usefulness, hydraulic modeling is subject to several limitations and sources of uncertainty:

- The accuracy and resolution of input data (e.g., Digital Elevation Models, land use, Manning's roughness coefficients).
- Model simplifications and assumptions (e.g., boundary conditions, friction laws).
- Parameter sensitivity and calibration issues (**Pappenberger et al., 2005**).

Therefore, model calibration and validation using observed data are critical steps to ensure the reliability of simulation outputs.

2.8 Software Used – HEC-RAS

To conduct hydraulic modeling of flood scenarios, this study employs HEC-RAS (Hydrologic Engineering Center – River Analysis System), a comprehensive software developed by the U.S. Army Corps of Engineers. HEC-RAS is a widely recognized tool for simulating 1D and 2D unsteady flow, flood inundation mapping, sediment transport, and water quality analysis.

This chapter provides an overview of HEC-RAS, its components, capabilities, and relevance to the study objectives. It also outlines the typical workflow used for hydraulic simulations in the software environment.

HEC-RAS is a free, open-access modeling tool designed to perform hydraulic calculations for natural and constructed channels. The software has evolved from a 1D steady flow simulator into a powerful platform supporting fully dynamic 1D/2D simulations with integration of GIS tools.

In 2D simulations, the domain is discretized into a mesh (regular or irregular). Each cell calculates flow based on depth-averaged Saint-Venant equations.

2.8.1 Key Modules:

- 1D Steady Flow: Gradually varied flow profiles in rivers and channels.
- 1D Unsteady Flow: Time-varying flows in river reaches and reservoirs.
- 2D Flow Modeling: Depth-averaged flow across floodplains or urban terrain.
- Sediment Transport: Simulation of bed changes due to sediment movement.
- Water Quality: Modeling temperature and constituent transport.

Brunner (2020) describes HEC-RAS as an industry-standard tool for flood risk analysis and river hydraulics.

2.8.2 HEC-RAS Advantages

HEC-RAS was chosen for this study based on several criteria:

- Accessibility: Free to download and supported globally.
- GIS Integration: Works directly with HEC-GeoRAS and RAS Mapper for terrain and spatial data.
- Flexibility: Supports both 1D channel flow and 2D floodplain modeling.
- Documentation and Community: Extensive user manuals, tutorials, and community support.

Moreover, HEC-RAS is accepted by regulatory agencies and used in numerous floodplain mapping and river engineering studies (**USACE, 2020**).

2.8.3 Key Components Used by HEC-RAS

Geometry Data

- River centerline and cross-sections
- Bank stations
- Flow paths
- Terrain model (DEM)
- Storage areas and connections (if applicable)

Flow Data

- **Boundary conditions**: Inflow hydrographs, downstream rating curves

- **Initial conditions**: Stage or flow profiles at start time
- **Unsteady flow data**: Time series data defining the simulation

RAS Mapper

A powerful tool for:

- Importing terrain (DEM) and land use data
- Defining 2D flow areas
- Visualizing simulation results (depth, velocity, extent)

2.8.4 Numerical Solver in HEC-RAS

HEC-RAS uses an implicit finite difference scheme to solve the 1D and 2D Saint-Venant equations. This allows for greater numerical stability even with larger time steps.

The 2D solver in HEC-RAS is based on the finite volume method (FVM), using Godunov-type schemes for accurate handling of shocks and wetting-drying fronts (Brunner, 2020).

2.10.5 Workflow Summary

The general steps followed in this study using HEC-RAS are:

a. **Terrain Preparation**
   - Obtain and preprocess DEM using GIS tools
   - Import into RAS Mapper

b. **Geometry Setup**
   - Define river reaches, cross-sections, and 2D flow areas
   - Assign Manning's n values (roughness)

c. **Flow and Boundary Conditions**
   - Define inflow hydrographs and downstream boundary types

d. **Simulation Parameters**
   - Set time step, duration, and numerical options
   - Run the unsteady flow analysis

e. **Result Analysis**
   - Use RAS Mapper to generate depth maps, velocity fields, and flood extents

- Export results for mapping or further analysis

2.8.5 Limitations of HEC-RAS

While powerful, HEC-RAS has certain constraints:

- Limited in handling highly 3D flow phenomena such as vortices or turbulence.
- Mesh generation in complex urban environments may require manual refinement.
- Requires high-quality terrain data for accurate 2D results.

Nonetheless, its versatility and ease of use make it an excellent choice for flood modeling in riverine and semi-urban settings.

Conclusion

This thesis explored the process of flood simulation and hydraulic modeling, focusing on the use of HEC-RAS software for flood risk assessment and management. We began by examining the importance of hydraulic modeling in predicting and managing flood events, which plays a crucial role in planning and infrastructure design. The mathematical foundation of flood modeling was introduced, with a focus on the Saint-Venant equations, which describe the unsteady flow in open channels and serve as the backbone for many hydraulic simulations.

We then looked at different numerical methods used to solve these equations, particularly finite difference and finite volume methods, which allow us to approximate solutions to complex flow problems. The study also compared different types of hydraulic models—1D, 2D, and 3D—each suited to different flow scenarios. While 1D models are used for simpler river or channel flow, 2D and 3D models offer greater detail and are particularly useful for simulating floodplain dynamics and more complex flow patterns.

The final part of the thesis focused on HEC-RAS, a widely used software for hydraulic modeling. HEC-RAS was chosen for this study because of its versatility, ease of use, and ability to simulate both 1D and 2D unsteady flows. It integrates with GIS tools, making it particularly effective for floodplain mapping and risk analysis. The software's workflow was outlined, from inputting geometry and flow data to running simulations and analyzing results.

In conclusion, this thesis demonstrates how hydraulic modeling and simulation tools like HEC-RAS are essential for understanding flood behavior, assessing risks, and supporting decision-making in flood management. The work also highlights the importance of selecting the right modeling approach based on the complexity of the problem and available data. The methods

explored here provide a strong foundation for improving flood prediction and mitigation strategies in the future.

CHAPTER3

3 Presentation of the Study Area – El-Hamiz River Watershed

3.1 Introduction

The El Hamiz River Watershed is located in the northern part of Algeria, east of the capital city, Algiers. It lies within a semi-urban and semi-rural environment, playing a vital role in water supply, agriculture, and flood control in the region. The watershed extends across several communes and includes various landforms such as hills, valleys, and plains. Its strategic location and hydrological importance make it a key area for water resource management and environmental planning.

3.2 Study Area Location "El Hamiz River Watershed"

The study area focuses on the El Hamiz River Watershed, situated in the eastern part of the Mitidja Plain. This watershed encompasses both the El Hamiz and Réghaïa valleys and covers an approximate surface area of 432 km² at its outlet near Bordj El Bahri. Geographically, it belongs to the Tablat Atlas, which represents the western extension of the Djurdjura Massif, and is characterized by a dense hydrographic network, reflecting the relatively low impermeability of the surrounding terrain.

To the east, the watershed is bordered by the abrupt elevation of the Djurdjura Massif, marking the entry to Grande Kabylie, while to the south, it is delimited by Djebel Tames Guida, whose highest point reaches 1,138 meters and defines the watershed's southern ridge line. The basin is exposed to moisture-laden Mediterranean winds, which contribute to significant runoff. However, its flow regime is intermittent: dry during the summer and prone to intense, rapid flooding during the winter rainy season.

The El Hamiz watershed falls within the Wilaya of Algiers, a region particularly vulnerable to flood risks. This vulnerability highlights the urgent need for the rehabilitation and proper management of the Oued El Hamiz to protect human lives. The population density, estimated at around 1,300 inhabitants/km², is unevenly distributed, with denser settlements—often informal and poorly planned—located near marshy zones along the riverbanks, particularly in the El Hamiz area.

Hydrologically, the El Hamiz River is a continuation of the Oued Larbatache, which originates in the Blidean Atlas at an altitude of 1,138 meters on its southern slope. Its flow is regulated by the El Hamiz Dam and exits the mountainous region near Larbatache before heading north through the Mitidja Plain and eventually discharging into the Mediterranean Sea.

The Lower Mitidja Plain (Mitidja-Est) is a broad alluvial plain with an average width of 20 km, shared between the Wilayas of Algiers and Boumerdes (***Fig 3.1***). It is bounded to the south by the foothills of the Blidean Atlas and to the north by the Sahel strip, a narrow and rugged coastal zone overlooking the Mediterranean, where the city of Algiers is located.

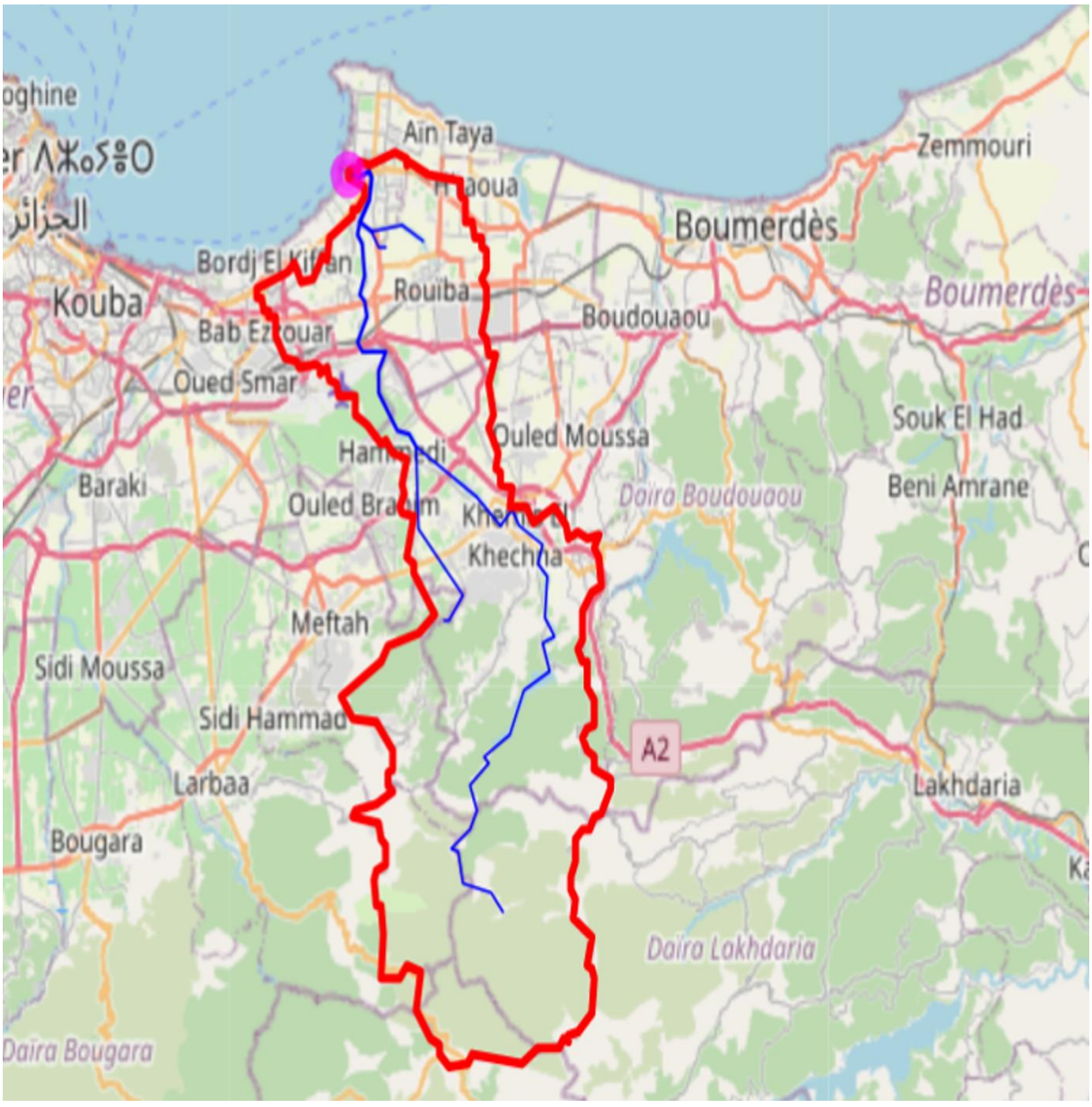

Fig 3.1. El Hamiz Watershed.

3.3 El-Hamiz Dam Characteristics :

The El-Hamiz Dam, located on the El Hamiz River in northern Algeria, is a strategically important hydraulic structure that serves multiple purposes, including flood control, irrigation, and urban water supply. Situated upstream of the eastern Mitidja Plain, near the town of

Larbatache, the dam is part of a broader effort to regulate surface water resources in a semi-arid region prone to seasonal hydrological variability (***Bouanani et al., 2017***).

Commissioned to address the recurrent flood risks and to ensure a reliable water supply to the growing population of Algiers and its eastern suburbs, the dam has a total storage capacity of around 22 million cubic meters (***ANRH, 2020***). It regulates inflows from the upper reaches of the El Hamiz watershed, capturing intense runoff during the rainy season (October–March) and releasing controlled flows during dry months, thus mitigating seasonal water shortages and supporting agriculture downstream (***Boudjemaa & Leduc, 2019***).

Structurally, the dam is a gravity-type dam with a combination of earthfill and concrete components, designed to withstand both hydraulic pressure and sediment loads originating from the highly erodible catchment. The watershed feeding into the reservoir is characterized by steep topography and variable land use, which results in a high sediment yield—a concern highlighted in multiple studies on dam sustainability in North Africa (***Mebarki et al., 2021***). Consequently, sedimentation has become a critical issue, gradually reducing the effective storage capacity of the reservoir and demanding regular sediment management strategies.

Table 3.1. Dam characteristics

Type		Gravity
Height (m)		50.00
Length (m)		222.00
Normal reservoir level (NRL) (m)		174.10
Maximum water level (MWL) (m)		175.00
Spillway :	Discharge (m^3/s)	930.00
	Crest elevation of the gate in closed position (m)	174.30
	Elevation of lower edge of gate at maximum open position (m)	172.80

Cylindrical gate	Elevation of lower edge of gate in closed position (m)	167.70
	Crest elevation (m)	169.00
Bottom outlet (m^3/s)		2 X 35

Moreover, evaporation losses, estimated at over 1,000 mm/year in the region (***Benmoussa et al., 2015***), further affect the dam's performance, especially during prolonged dry spells. These climatic constraints, compounded by increasing water demand due to urban expansion, necessitate integrated watershed and reservoir management approaches.

In summary, the El-Hamiz Dam plays a vital role in regional water security and flood protection, but its long-term effectiveness is challenged by sedimentation, climate variability, and anthropogenic pressures. Sustainable operation of the dam requires a coordinated effort involving hydrological monitoring, catchment management, and adaptive infrastructure planning (***UNESCO, 2022***).

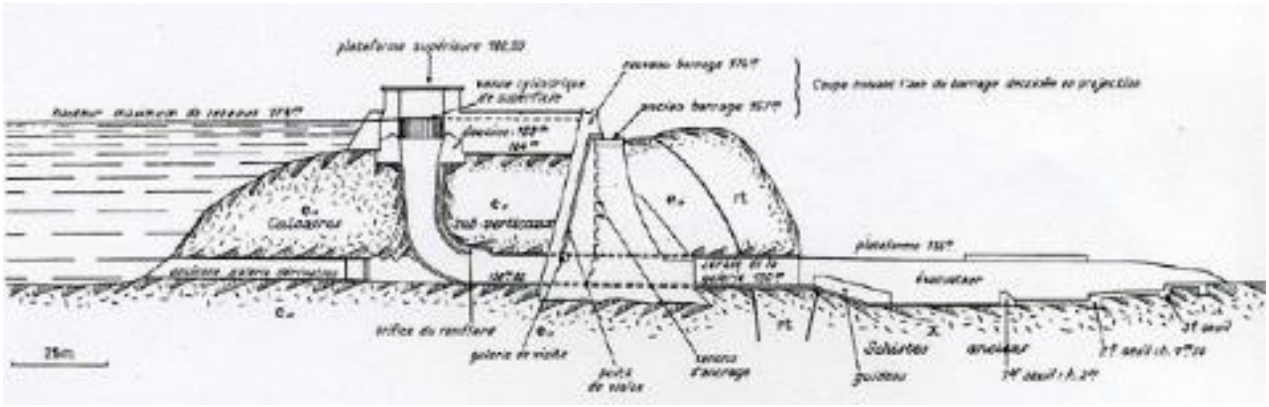

Fig 3.2. Cross section.

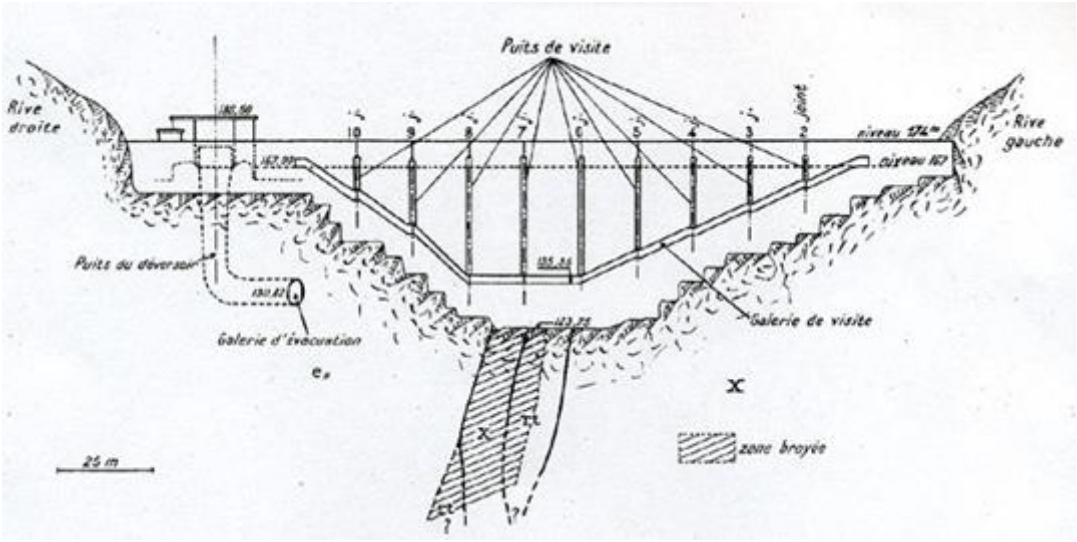

Fig 3.3. Longitudinal section.

3.4 Watershed Morphometric Characteristics

The El-Hamiz River Watershed, which spans an approximate area of 321 km², exhibits morphometric features that are essential in understanding its hydrological response, sediment transport, and flood potential. Morphometric analysis—based on quantitative evaluation of the watershed's shape, drainage pattern, and relief—provides key insights into runoff behavior, erosion susceptibility, and basin hydrodynamics (***Strahler, 1957; Schumm, 1956***).

The drainage network of the El-Hamiz basin is classified as tree-shaped, which indicates a relatively homogeneous lithology and moderate to low structural control over surface flow. The watershed is part of the Tablat Atlas foothills, where elevations range from over 1,100 meters in the southern uplands to near sea level at its outlet near Bordj El Bahri. The main channel length (El Hamiz River) is approximately 40 km, and the drainage density (Dd) of the basin is relatively high—estimated at around 2.8 km/km²—suggesting rapid surface runoff and limited infiltration (***Horton, 1945; Bouanani et al., 2017***).

The bifurcation ratio (Rb), which reflects the degree of branching in the drainage network, has been calculated in the range of 3.0 to 4.5, consistent with regions prone to flash floods, especially during intense Mediterranean rain events (***Mebarki et al., 2021***). Similarly, the form factor (Rf), which indicates basin shape, is relatively low (Rf < 0.5), implying that the basin is elongated and that peak flow arrives more gradually, but still with significant volume and energy when saturated.

Relief-related indices such as basin relief, ruggedness number, and hypsometric integral show the terrain's moderate to steep nature in upper catchments and a transition to flat areas in the

Mitidja plain, where urbanization and agricultural use dominate. These geomorphic transitions greatly influence flood risk zones, sediment yield, and hydraulic modeling parameters (***Nag & Chakraborty, 2003***).

Importantly, the steep upper sections, coupled with erodible lithologies, contribute to a high sediment load, which accelerates reservoir siltation in the El-Hamiz Dam. This interaction between morphometric properties and sediment dynamics is critical for sustainable watershed and dam management (***Boudjemaa & Leduc, 2019***).

3.4.1 Geological Characteristics

The El-Hamiz River Watershed lies within the complex geotectonic framework of northern Algeria, specifically within the Tellian Atlas system, which forms part of the larger Algerian Alpine Belt. The geology of the watershed plays a crucial role in determining the hydrological response, sediment yield, and land stability, all of which influence flood behavior and watershed management strategies (***Belhai, 2006; Derradji et al., 2014***).

The southern part of the watershed is dominated by the Blidean Atlas, composed primarily of Mesozoic and Cenozoic sedimentary formations, including limestones, marls, and sandstones, which are moderately consolidated and prone to erosion, especially on steep slopes. The northern section, transitioning toward the Mitidja Plain, consists of more recent Quaternary alluvial deposits, characterized by gravel, sand, silt, and clay, deposited by fluvial activity over time (***Remini, 2011***).

These unconsolidated alluvial deposits are highly permeable, enabling significant infiltration and temporary groundwater storage, but they also increase the susceptibility to subsurface instability and soil liquefaction during intense rainfall or seismic activity. Moreover, the transition from high-relief lithological units in the south to flat, sediment-laden zones in the north makes the area particularly vulnerable to sediment transport and deposition, which contributes to the rapid siltation of hydraulic structures such as the El-Hamiz Dam (***Mebarki et al., 2021***).

Structurally, the watershed is influenced by north-south and northeast-southwest fault systems, remnants of compressive tectonic activity associated with the convergence between the African and Eurasian plates. These tectonic features not only shape the topography but also contribute to landslide susceptibility, particularly in zones with weak lithology and deforested slopes (***Benhamza et al., 2020***). Understanding the geological composition and structural controls of the El-Hamiz basin is essential for predicting erosion patterns, planning sustainable land use,

and ensuring the stability of critical infrastructures such as dams, bridges, and urban developments located downstream.

3.4.2 Land Use / Land Cover Characteristics

The El-Hamiz River Watershed features a diverse pattern of land use and land cover (LULC), which significantly influences its hydrological behavior, erosion dynamics, and flood vulnerability. The spatial distribution of vegetation, urban development, and agricultural activities within the basin is a direct result of both natural topography and anthropogenic pressures, especially those related to rapid urbanization near the capital city, Algiers (***Bouanani et al., 2017; Remini, 2011***).

Using recent satellite imagery and GIS-based classification, the LULC in the watershed can be broadly categorized into five main types:

Urban areas: Concentrated primarily in the lower northern parts of the basin, particularly around El Hamiz, Bordj El Bahri, and adjacent sectors of the Mitidja Plain. These urban zones have expanded rapidly over the past two decades due to population growth, often in an unplanned and informal manner. This expansion has reduced infiltration capacity and increased surface runoff, exacerbating flood risk (***UN-Habitat, 2020***).

Agricultural land: Agriculture dominates the central and northern parts of the basin, especially along flatter terrain in the Mitidja Plain. These areas include both irrigated and rainfed croplands, particularly cereals, vegetables, and orchards. While agriculture contributes positively to local economies, intensive cultivation often results in soil compaction, fertilizer runoff, and erosion, particularly in sloping areas (***Boudjemaa & Leduc, 2019***).

Forest and shrubland: Found primarily in the southern and southeastern uplands, where elevation and slope are higher. These vegetated zones play a crucial role in reducing surface runoff, stabilizing soils, and regulating local climate. However, deforestation due to wood harvesting and land clearing has led to a decline in these protective covers, aggravating sediment yield into the El-Hamiz Dam (***Mebarki et al., 2021***).

Bare or degraded land: Typically observed in eroded hillslopes and construction zones, where vegetation cover has been removed. These zones exhibit high runoff coefficients and are major contributors to sediment transport, especially during heavy rain events.

Water bodies: Including the El-Hamiz Reservoir and intermittent water channels, which vary seasonally depending on rainfall. These features play a key role in water storage and distribution but are directly impacted by upstream land use practices and sedimentation rates.

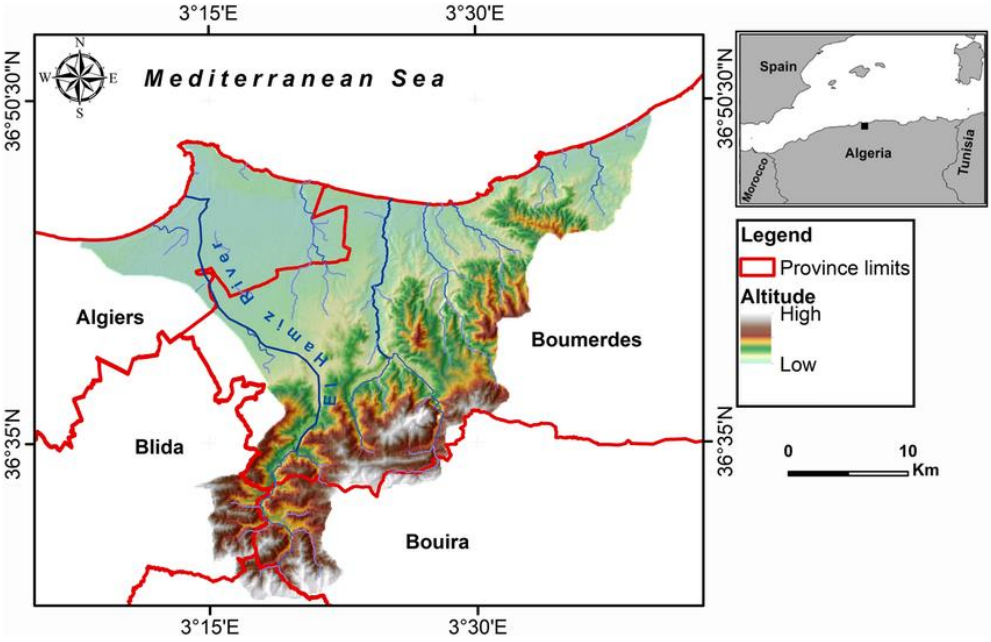

Fig 3.4. Carte de localisation du bassin versant de l'Oued El Hamiz (Blida, Bouïra, Boumerdès, Alger, Algérie) • Adapté de *Nemer et al.* (2023).

Overall, the land use configuration in the El-Hamiz Watershed reflects a dynamic and evolving landscape, where urban sprawl, agricultural intensification, and land degradation present significant challenges to hydrological stability and ecosystem resilience. Sustainable land management strategies—such as afforestation, soil conservation, and urban planning regulations—are urgently needed to preserve watershed function and reduce downstream flood hazards (***FAO, 2015***).

3.4.3 Climatic Characteristics :

The El-Hamiz River Watershed, located in the northeastern Tellian region of Algeria, is characterized by a Mediterranean climate typified by hot, dry summers and mild, wet winters. This climatic pattern directly influences runoff generation, soil erosion, vegetation dynamics, and flood occurrence, especially given the topographical contrasts between the upland and lowland zones of the basin (***Meddi & Hubert, 2003; Boudjemaa & Leduc, 2019***).

The watershed's climate is controlled by both altitudinal variation and proximity to the Mediterranean Sea, resulting in spatial variability in precipitation, temperature, and evapotranspiration. Higher elevation zones in the south of the watershed tend to receive more

rainfall and experience lower average temperatures, while the lower northern plains are warmer and drier, especially during the summer months.

Table 3.2: Climatic data observed at the Dar El Beida station (1975–2010)

Monthly average	Sep	Oct	Nov	Dec	Jan	Feb	Mar	Apr	May	June	July	Aug
Precipitation (mm)	28	65	103	94	79	74	53	58	46	7	4	13
Temperature (°C)	23.3	13.3	15	12.1	10.9	11.3	13.3	15.1	18.9	22.8	25.5	26.2
Wind speed (m/s)	2.5	2.1	2.4	2.5	2.3	2.4	2.4	2.8	2.7	2.9	2.8	2.6
Sheltered evaporation (mm)	105	80	66	55	55	49	65	78	84	106	122	127

3.4.4 Precipitation Regime

Precipitation in the El-Hamiz watershed is seasonal and highly variable, with approximately 75–80% of annual rainfall occurring between October and March. Mean annual precipitation ranges from 600 mm to 900 mm, depending on altitude and exposure to moisture-laden winds from the sea. However, the watershed is prone to short, intense rainfall events, often associated with convective storms, which contribute to flash flooding and rapid surface runoff ***(Meddi et al., 2010; Bouanani et al., 2017***). Such events are particularly dangerous in urbanized areas like El Hamiz, where impervious surfaces prevent infiltration, exacerbating peak discharge volumes. Moreover, climate variability and climate change projections suggest increasing extremes in rainfall patterns, posing additional challenges for flood risk management (**Driouech et al., 2009**).

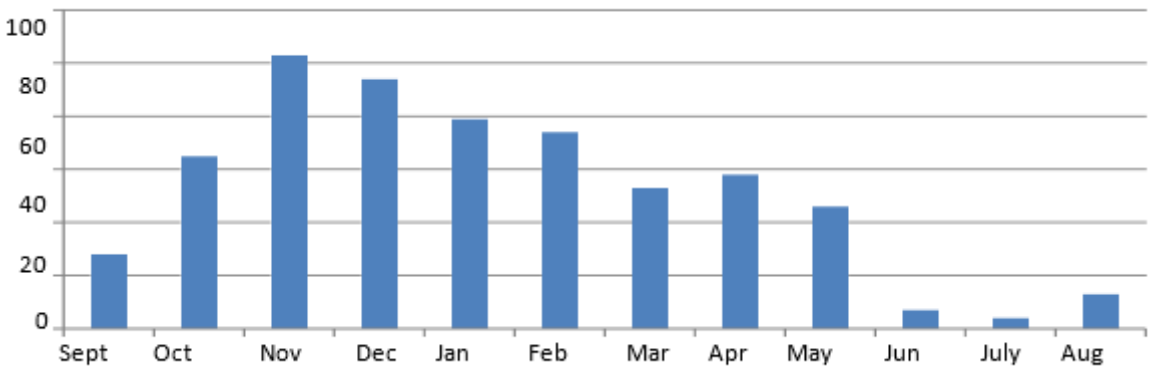

Fig. 3.5: Distribution of average monthly precipitation.

3.4.5 Temperature Regime

Temperature variations follow a typical Mediterranean profile, with average monthly temperatures ranging from 10–12°C in January to 28–32°C in July and August. The watershed experiences high summer evapotranspiration rates, which, coupled with reduced precipitation, leads to a dry season water deficit, especially affecting agricultural productivity and surface water availability (***ONM, 2022***).

The diurnal temperature range is also significant, particularly in elevated regions, influencing soil moisture dynamics and vegetation cover. These temperature patterns must be considered when calibrating hydrological models and estimating actual evapotranspiration.

3.4.6 Other Relevant Climatic Variables

The watershed's potential evapotranspiration (PET) values, estimated using the Penman-Monteith method, range from 900 mm/year to 1200 mm/year, depending on elevation, land cover, and season (***FAO, 1998***). These high PET values, particularly in summer, reduce effective rainfall, further stressing surface water and groundwater resources.

Wind patterns also influence local climate, especially northeasterly maritime winds that bring moisture and contribute to orographic precipitation in the southern hills. On the other hand, dry continental winds from the Sahara can occasionally raise temperatures and increase fire risk in vegetated areas.

3.4.7 Hydrological Characteristics

The El-Hamiz River Watershed presents a complex hydrological regime shaped by its Mediterranean climate, steep topography, land cover heterogeneity, and human interventions such as dam construction and urbanization. Understanding the hydrology of the basin is critical

for designing flood mitigation strategies and for implementing integrated watershed management approaches.

Table 3.3. Main hydrological characteristics of the El Hamiz watershed

Characteristic	Value	Notes / Source
Location	Northeastern Mitidja, Algeria	Wilaya of Algiers and Boumerdès
Surface Area	≈ 432 km²	Source: ANRH reports, local watershed studies
Main River	Oued El Hamiz	Tributary of the Mediterranean Sea
Length of Main Stream	≈ 45 km	Estimated from GIS and hydrological databases
Altitude Range	~40 m to 900 m	From downstream plains to upstream hills
Average Slope	~6%	Based on DEM analysis
Climate Type	Mediterranean	Mild, wet winters and hot, dry summers
Average Annual Rainfall	600 – 900 mm/year	Source: ONM (Office National de la Météorologie), varies by elevation
Temperature Range	5°C (winter) to 35°C (summer)	Regional climate data
Geology	Alluvial plains, marls, schists	Source: BRGM & local geological surveys
Land Use	Urban, agricultural, forested	Land cover analysis based on satellite imagery (e.g., CORINE, Landsat)
Soil Type	Clay, loam, sandy-clay	Affects infiltration and runoff behavior
Main Flood Risks	Flash floods, urban runoff	Due to urban expansion and steep slopes in upstream zones

3.4.8 Surface Runoff and Streamflow

The basin experiences a marked seasonality in flow patterns, typical of Mediterranean regions. During the wet season (October–March), heavy and often intense rainfall events produce high runoff coefficients, particularly in the urban and bare-soil zones where infiltration is limited. Consequently, flash floods are common, especially in the lower basin near El Hamiz and Bordj El Bahri. In contrast, during the dry season (May–September), streamflow diminishes

drastically, with many tributaries becoming intermittent or completely dry (***Meddi & Hubert, 2003; Bouanani et al., 2017***).

The streamflow is also strongly influenced by the presence of the El-Hamiz Dam, which regulates the flow regime downstream. While the dam helps in mitigating peak flood discharges during high rainfall periods, its storage capacity is threatened by sediment accumulation from upstream erosion, a phenomenon exacerbated by land degradation and deforestation (***Mebarki et al., 2021***).

3.4.9 Flood Behavior and Risk

Historical flood events in the watershed have demonstrated the basin's vulnerability, particularly in urban areas with inadequate drainage infrastructure. The 2001 and 2018 flood events, for example, resulted in significant economic damage and exposed weaknesses in stormwater management systems and urban planning practices (***Remini, 2011***).

The hydrograph of the El-Hamiz River is typically characterized by sharp rising limbs and steep recession curves, indicating rapid surface runoff and limited baseflow contributions. This hydrological behavior demands the implementation of early warning systems and nature-based solutions (e.g., reforestation, permeable surfaces) to improve water retention in the basin.

Table 3.4: Inventory of floods at the El Hamiz Dam

Date	Maximum discharge (m^3/s)	Flood volume (Mm^3)	Rainfall (mm)
21 November 1957	690	–	–
13–14 April 1954	660	5	150 mm in 24 hours; 95 mm in 6 hours
26–27 February 1939	520	10	–
11–12 December 1935	510	–	128 mm in 24 hours
29–30 December 1957	420	24	126 mm in 30 hours
15–16 April 1939	400	9	–

18 February 1939	360	16	–
21 May 1921	300	–	93 mm in 3 hours
8–9 April 1939	280	10	–
8–10 April 1954	Several floods: 230, 310, 300	28	230 mm in 48 hours
7 April 1965	180	4.8	45 mm in 10 hours

3.5 Groundwater Interaction :

Although primarily a surface-water-driven basin, the Mitidja Plain aquifer, located in the northern part of the watershed, interacts with the river system in terms of recharge and discharge. Infiltration from agricultural zones and floodplains contributes to the shallow aquifer, especially during wet years. However, over-extraction of groundwater for urban and agricultural uses has led to drawdown of water tables, which in turn reduces baseflow during dry periods and exacerbates water scarcity (***Derradji et al., 2014***).

3.6 Conclusion :

The El-Hamiz River Watershed, located in the eastern sector of the Mitidja plain in northern Algeria, represents a hydrologically and geomorphologically complex system. Encompassing an area of approximately 321 km², the watershed is characterized by marked altitudinal gradients, a dense hydrographic network, and heterogeneous landforms shaped by the interaction between the Djurdjura Massif to the south and the coastal plains to the north. The El-Hamiz Dam constitutes a critical hydraulic infrastructure within the basin, providing flood regulation and water supply services, yet facing operational limitations due to sedimentation and land degradation in its upstream catchment.

Morphometric parameters indicate a predisposition to rapid runoff and flash flooding, particularly under intense rainfall conditions typical of the region's Mediterranean climate. Geologically, the basin is underlain by alluvial and sedimentary formations of varying permeability, influencing both surface and subsurface hydrological processes. Land use within the watershed reflects a growing trend of urbanization and agricultural intensification, often in conflict with sustainable watershed management principles. Climatic conditions are dominated by pronounced seasonality, with wet winters and arid summers, leading to significant temporal variability in hydrological responses.

Hydrologically, the basin exhibits a predominantly ephemeral flow regime, with peak discharges occurring during short, intense rainfall events, and limited baseflow contributions

during dry periods. Groundwater-surface water interactions remain modest and increasingly strained by overexploitation. Collectively, these characteristics highlight the watershed's sensitivity to both natural and anthropogenic pressures, and underscore the urgent need for integrated water resource management strategies. The comprehensive analysis presented herein provides a critical foundation for advanced hydrological modeling and informed decision-making in flood risk mitigation and sustainable development planning.

CHAPTER 4

4 Floods simulation in El-Hamiz Watershed via HEC RAS

4.1 Introduction

Floods are among the most frequent and devastating natural hazards worldwide, often resulting in significant human and material losses. In recent decades, their occurrence has been exacerbated by rapid urbanization, land use changes, and the growing impacts of climate change. These factors have heightened the need for robust tools to assess and manage flood risks, particularly in vulnerable regions.

The El Hamiz watershed, located east of Algiers, is one such area highly susceptible to flooding. Its topographical characteristics, coupled with dense and often unregulated urban development, contribute to the increased likelihood of severe flood events. Recent episodes of intense rainfall have exposed the limitations of the existing drainage infrastructure and underscored the urgency of comprehensive flood risk analysis in this watershed.

In this context, hydraulic modeling serves as a critical decision-support tool. It enables the simulation of flood events, the identification of high-risk zones, and the evaluation of potential mitigation strategies. Among the available tools, the HEC-RAS software (Hydrologic Engineering Center – River Analysis System), developed by the U.S. Army Corps of Engineers, is widely recognized for its capacity to model one- and two-dimensional free-surface flow in rivers and channels.

This chapter focuses on the application of HEC-RAS to simulate flood scenarios within the El Hamiz watershed. The objective is to analyze the hydraulic behavior of the area during extreme hydrological events, delineate flood-prone zones, and generate data that can inform future planning and risk management efforts.

4.2 Data Requirements for HEC-RAS Simulation

The simulation requires several inputs. Key datasets include:

A Digital Elevation Model (DEM), which was obtained from the USGS website. This dataset provides ground elevation data for the study area.

Peak flow rates and hydrographs. These can be acquired directly from hydrometric stations or derived using hydrological methods, as discussed in the following sections.

4.3 Peak flow calculation

The peak flow of the watershed was estimated using several empirical formulas:

4.3.1 Method of SCS Dimensionless Unit Hydrograph

The SCS Dimensionless Unit Hydrograph, established by the U.S. Soil Conservation Service (**Mockus, 1964**), is a practical method used to derive direct runoff hydrographs from excess rainfall, particularly in ungauged basins. It applies a standardized, dimensionless shape that can be scaled using watershed-specific parameters like lag time and peak flow.

According to Mishra and Singh (2003), this method has proven effective for small to medium-sized watersheds, especially when combined with the SCS Curve Number approach for estimating excess rainfall. However, they emphasize that local calibration may improve its accuracy in different climatic or physiographic conditions.

The method's ease of use and minimal data requirements have contributed to its widespread adoption, and it remains integrated into modern hydrologic tools such as HEC-HMS and HEC-RAS.

$$Qp = [\,2.08 * A/Tp] * \ P \qquad (4.1)$$

Qp : peak flow (m3/s) ; A: watershed area (km²); P: precipitation (cm); Tp: time to peak.

Qp= 57.48 m3/s

4.3.2 Giandotti Formula :

The Giandotti formula is an empirical method developed in Italy for estimating the concentration time (Tc) of a watershed, which is a critical parameter in hydrological modeling. The formula is particularly suited to small and medium-sized catchments with varied topography and land use.

As noted by Coppola et al. (2017), the Giandotti formula provides reasonably accurate estimates of concentration time in Mediterranean and Alpine environments, especially when detailed data are scarce. However, its empirical nature requires careful application and possible calibration outside of the regions for which it was originally developed.

Due to its simplicity and low input data requirements, the formula is often used in preliminary hydrologic assessments and is compatible with rainfall-runoff models such as those implemented in HEC-HMS and HEC-RAS.

$$\boldsymbol{Q_p = \frac{C \times A \times H_T \times \sqrt{H_{men} - H_{min}}}{4 \times \sqrt{A} + 15 \times L}} \qquad (4.2)$$

C: topography coefficient [66, 166] (for Giandotti); A: Watershe area (km²); H_T: precipitation (m); H_{mean}: mean elevation; $H_{min:}$ min elevation; Length of the watercourse (km).

$$Qp= 20.08\ m^3/s$$

4.3.3 Mallet- Gauthier formula :

The Mallet–Gauthier formula is a classical empirical equation used to estimate the peak flow of a watershed. It is commonly applied in French and North African hydrological studies due to its simplicity and suitability for rural and semi-urban catchments.

As highlighted by Remini and Achour (2009), the Mallet–Gauthier formula is well-adapted to North African hydrological contexts, where limited gauged data often necessitate the use of empirical models. While it does not consider land use or soil characteristics explicitly, it remains valuable for initial hydrological assessments.

Due to its low data requirements and ease of computation, this formula is frequently used in preliminary design and flood modeling studies, especially where detailed topographic and hydrologic information is not available.

$$Q_p = 2 \times k \times \ln(1 + 20 + H) \times A \times \sqrt{\frac{1+4\times\ln T-\ln A}{L}} \qquad (4.3)$$

Where, k: coefficient from 0.5 to 5; H: yearly precipitation (m); T: return period (year).

$$Qp= 553.65\ m^3/s \text{ (For T=100 years)}$$

4.3.4 Possenti formula :

The Possenti formula is an empirical method used in small to medium-sized watersheds. It was originally developed in Italy and is particularly applicable in mountainous and Mediterranean regions, where hydrological responses are often rapid due to steep slopes and short flow paths.

As discussed by De Michele and Salvadori (2002), the Possenti formula provides a good approximation for Mediterranean basins, especially where rainfall-runoff processes are dominated by fast hydrological responses. However, it is important to consider that, like other empirical formulas, its accuracy can vary outside the climatic and geomorphological context for which it was derived.

$$Q_p = \frac{C\cdot P}{L(A_m+\frac{S_f}{3})} \qquad (4.4)$$

C morphological coefficient 700<C<800; P: precipitation (mm); L: watercourse length (km); Am: mountainous area (km); flat area (km).

$$Qp= 136.50\ m^3/s$$

4.3.5 Iskovski Formula

The Iskovski formula is an empirical approach developed primarily for use in Eastern European hydrological contexts, particularly in small to medium-sized watersheds. Which is essential for modeling flood response and runoff generation.

According to Todorovic and Maksimovic (1987), the Iskovski formula performs well in hilly or mountainous terrains where terrain slope and channel length significantly influence runoff timing. It is especially suited for initial design in ungauged catchments, where limited data restrict the use of more physically based models.

Despite being less commonly used than other European formulas, its simplicity and regional accuracy make it valuable for flood estimation studies in similar geographic conditions and for integration into models such as HEC-HMS or HEC-RAS.

$$Qp = n.m.Pv.A \quad (4.5)$$

n and m morphologic coefficients; Py: yearly precipitation (m); watershed area (km²).

$$Qp= 150.95\ m^3/s$$

4.3.6 Turazza Formula

The Turazza formula is an empirical equation developed in Italy for estimating the time of concentration (Tc) in small and medium-sized catchments. It is particularly suited for regions with complex topography and limited hydrological measurements, such as the Mediterranean basin.

As noted by Versace et al. (2001), the Turazza formula has been widely applied in Italian hydrology due to its simplicity and reliability in mountainous and hilly terrain.

Although empirical, the formula remains useful for preliminary hydrological assessments and is compatible with common modeling tools like HEC-HMS, where quick Tc estimates are needed for flood simulation.

$$Q_p = \frac{1}{3.6} C.i_{max}.A \quad (4.6)$$

C: coefficient; Imax: precipitation intensity (mm/h); A: watershed area (km²).

Qp= 138.18 m^3/s .

4.3.7 Sokolovsky Formula

The Sokolovsky formula is an empirical method originally developed in the Soviet Union to estimate the peak flow in watersheds, particularly those characterized by variable slopes and mixed land cover. It remains relevant in hydrological studies across Eastern Europe and similar regions.

Sokolovsky (1968) proposed this formula based on a statistical analysis of observed runoff responses in various Russian catchments. Later studies, such as those by Gartsman (2008), confirmed its utility in catchments with rapid hydrological reactions and limited field data, making it suitable for flood modeling in ungauged basins.

Due to its adaptability and ease of use, the Sokolovsky formula is often used for preliminary flood assessments and is compatible with hydrologic simulation tools like HEC-HMS.

$$Q_p = \frac{0.28 \times P_{tc} \times C_r \times S \times F}{T_m} \quad (4.7)$$

F: Flood shape coefficient; a: Flood runoff coefficient for a given period; Ptc: short-term frequent rainfall corresponding to the concentration time; Tc: concentration time[h]

Qp= 96.32 m^3/s

In this study, the peak discharge is determined using the Mallet–Gauthier formula, as it yields the highest value among the evaluated methods, thus representing the most critical (worst-case) flood scenario. Accordingly, the peak flow is taken as **Qp=553.65m³/s**.

To incorporate the capacity of the dam's spillway during flood events, a discharge rate of **394.5 m³/s**—corresponding to a 100-year return period and based on prior studies—is added. This results in a total peak flow rate of **Qp = 948.12 m³/s**.

4.4 Calculation of the time of concentration

The time of concentration (Tc) is a critical parameter for developing the watershed's runoff hydrograph. Similar to the peak flow analysis, several empirical formulas were applied to estimate Tc:

4.4.1 Soil Conservation Service (SCS) Formula

The SCS formula estimates TcTc using watershed geometry. While SCS methodologies are widely applied in ungauged catchments, this specific formula prioritizes topographical parameters..

$$T_c = \left(\frac{0.87 \times L^3}{H_{Max} - H_{Min}}\right)^{0.385} \quad (4.8)$$

Where: L = main channel length (km), Hmax = maximum elevation (m), Hmin= minimum elevation (m).

T_c= 10.39 h .

4.4.2 Giandotti Formula

This formula integrates area, channel length, and relief to estimate runoff response time, particularly in Mediterranean regions..

$$T_c = \frac{4\sqrt{S} + 1{,}5L}{0{,}8\sqrt{H_{Mean} - H_{Min}}} \quad (4.9)$$

Where: A= watershed area (km²), Hmean = mean elevation (m)

Tc= 14.74 h

4.4.3 Kirpich Formula

Developed for rural/mountainous basins, Kirpich's formula relies on channel slope and length..

$$T_c = 0{,}6616 \cdot L_p^{0{,}77} \cdot i_{mean}^{0{,}385} \quad (4.10)$$

Where: i_{mean} = mean channel slope (m/m)

Tc= 7.01 h

4.4.4 Ventura Formula

Tailored for Mediterranean basins, Ventura's method uses watershed slope and rainfall intensity.

$$T_c = 0{,}1272 \sqrt{\frac{S}{i_{mean}}} \quad (4.11)$$

S = watershed slope (m/m), imean = mean rainfall intensity (mm/h)

Tc= 3.83 h

A shorter time of concentration intensifies flood severity by amplifying peak discharge rates. The Ventura formula yielded the lowest value (Tc=3.83h), representing a conservative (worst-case) scenario for flood modeling.

4.5 Establishment of the hydrograph flow

HEC-RAS requires initial and boundary conditions, including upstream liquid inflow data for the wadi (river channel). As observed flood hydrographs were unavailable, the Sokolovsky method was selected for synthetic hydrograph generation. This approach is particularly suitable for Saharan regions and operates using two key parameters: peak discharge (Q_p) and time of concentration (Tc).

4.5.1 Flood Hydrograph Characteristics

A flood hydrograph (hydrograph flow) represents the watershed's hydrological response, typically exhibiting an asymmetrical bell-shaped curve divided into four phasesc (**Bouach, 2011**):

- Recession (prior to net rainfall)
- Rising limb (flood onset)
- Falling limb (recession)
- Baseflow recovery (post-event)

Key temporal parameters include (**figure 4.1**):

- Basin response time (t_p)**:** Time between the centroid of net rainfall and peak discharge.
- Time of concentration (T_c)**:** Travel time for water from the hydrologically most distant point to reach the outlet (T_c = 3.83 h for this study).
- Rising time (t_m)**:** Duration from initial rapid flow arrival to peak discharge ($t_m \approx$ Tc).
- Base time (t_b)**:** Total duration of direct runoff.

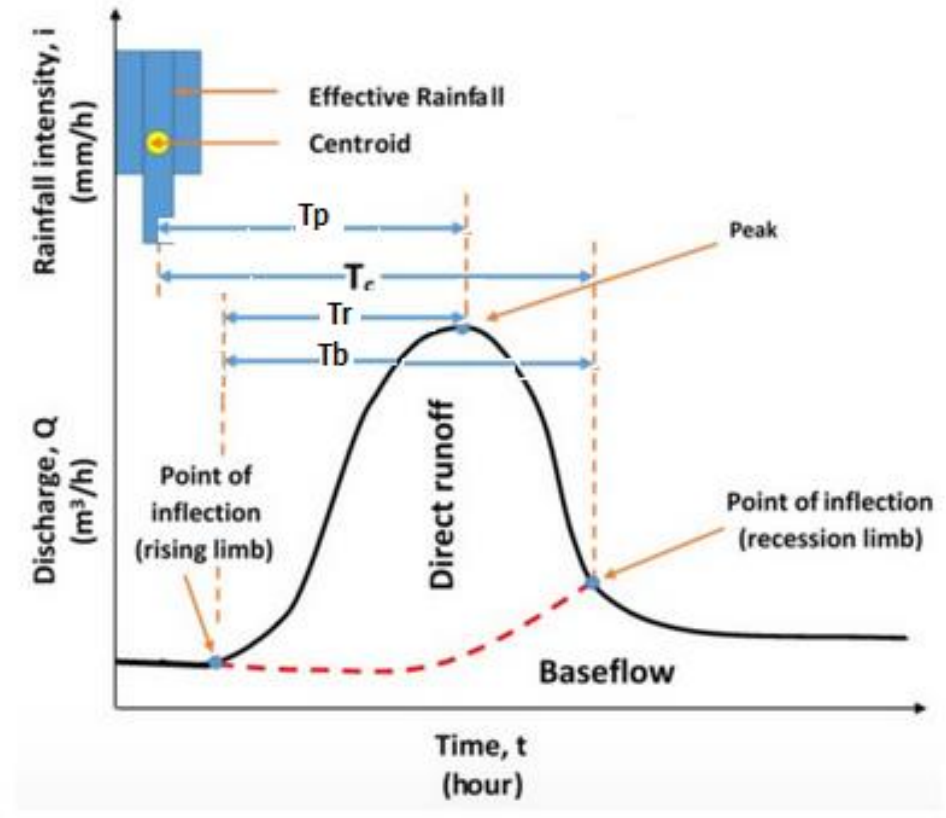

Fig 4.1: Description of the flood hydrograph (**Alamri et al., 2023**).

4.5.2 Sokolovsky Formulation

The method divides the hydrograph into rising and falling limbs, each modeled with parabolic equations scaled to peak flow and concentration time (**Bouach, 2011**)::

- **Rising Limb : (t < tr)**

$$Q_t = Q_p \left(\frac{t}{t_r}\right)^2 \quad (4.12)$$

- **Falling Limb : (t > tr)**

$$Q_t = Q_p \left(\frac{t_r - t'}{t_d}\right)^3 \quad (4.13)$$

Where:

- $t' = t - t_r$
- $t_d = \gamma \cdot t_r$
- γ= watershed coefficient (typically 2.0–3.0 for arid regions)

The resulting hydrograph (see **Figure 4.2**) provides critical upstream boundary conditions for HEC-RAS simulations

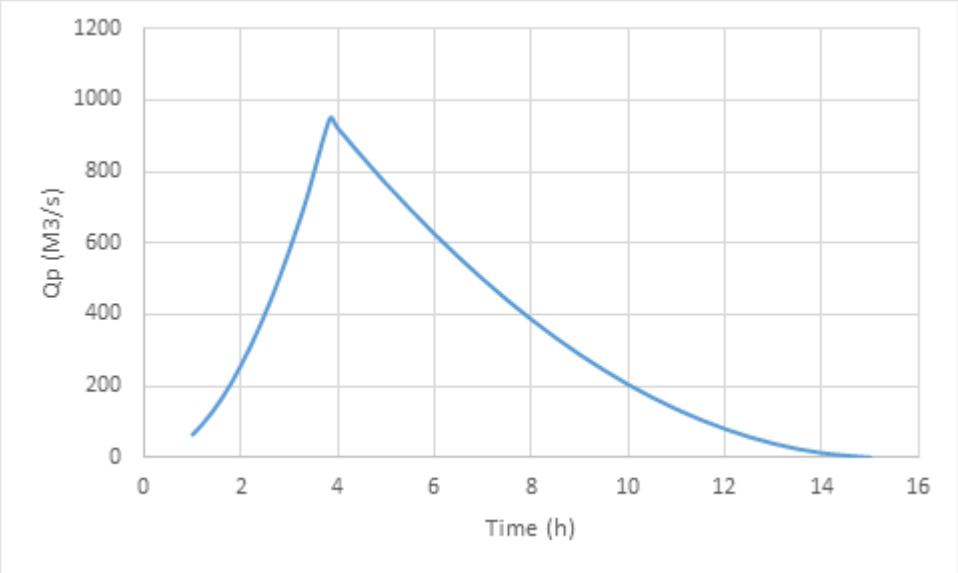

Fig 4.2: Estimated hydrograph flow of El Hamiz Watershed

4.6 Simulation with Hec-Ras

To study the hydrological response of the Hamiz watershed, we used HEC-RAS software. We used two types of simulation:

4.6.1 Steady Flow Simulation

in HEC-RAS assumes that the flow conditions (discharge, water level, velocity) do not change over time. It is like taking a snapshot of the river under a fixed flow rate. It is useful for analyzing design floods, water surface profiles, and checking channel capacity.

4.6.2 Unsteady Flow Simulation

models flow that changes with time. It shows how water levels and velocities evolve during a storm or flood event (e.g., hour by hour). It is more realistic and used for flood forecasting, dam break analysis, and hydrograph routing.

Table 4.1: Differences between steady and unsteady simultation in HEC RAS

Feature	Steady Flow Simulation	Unsteady Flow Simulation
Flow condition	Constant in time	Changes with time
Use case	Simple flood analysis, design checks	Detailed flood modeling, flood wave movement
Input	Single flow rate or profile	Hydrograph (flow vs. time)
Computation	Faster, less data needed	Slower, needs more data and calibration
Result type	Static (one result per location)	Dynamic (time series of results)
When to use	For design discharge or floodplain mapping	For simulating flood duration and peak timing

4.6.3 Steady flow Simulation Analysis

The most critical variables to analyze in flood studies are water depth and flow velocity. In the following section, we examine these two parameters in detail across the entire watershed.

4.7 Analysis of the water depth map

In HEC-RAS steady-flow simulations, the hydraulic behavior of a river reach is defined by three fundamental elements: (1) a series of cross-sections—vertical "slices" of the channel and floodplain (shown in green)—which capture local geometry for computing flow area, wetted perimeter, and hydraulic radius; (2) the river centerline (shown in blue), connecting these cross-sections along the primary flow path and establishing stationing; and (3) bank stations (marked in red), delineating boundaries between the main channel and left/right overbank areas, enabling distinct roughness coefficients and flow properties to be applied. Collectively, these components establish the conceptual framework for applying upstream and downstream boundary conditions, facilitating the calculation of steady-state water surface profiles and velocity distributions. The following section presents a detailed analysis of model outputs—water surface elevations, flow depths, and energy gradients—interpreted within this geometric and hydraulic framework (**Figure 4.3).**

The steady simulation results demonstrate the impact of the peak flow scenario (a 100-year return period). These results indicate that Wadi El Hamiz flooded both banks along its entire length, with severe flooding occurring in the following areas (Figure 4.3):

- Ben Ammar area (between cross-sections 14146 and 10778), located on the eastern bank. Floodwaters inundated several residential neighborhoods.
- Eastern runway area of Houari Boumediene International Airport (between cross-sections 10778 and 8694). Floodwaters covered a significant portion of this zone.
- El Hamiz city along National Road No. 5 (between cross-sections 8694 and 6808), where neighborhoods on the valley's western side were flooded.
- Bordj El Bahri, a densely populated city where floodwaters reached the western bank up to the valley's outlet into the Mediterranean Sea.

Flooding in these areas correlates with topographical characteristics. The terrain exhibits notably flat topography, as evidenced by cross-section profiles in these zones (see **Annex A figures**).

One explanatory factor is the reduced flow velocity in these areas (**Figure 4**.4 and **Table** A1 in **Annex** A), attributable to the valley channel's gentle slope (**Figure A6 in Annex A**).

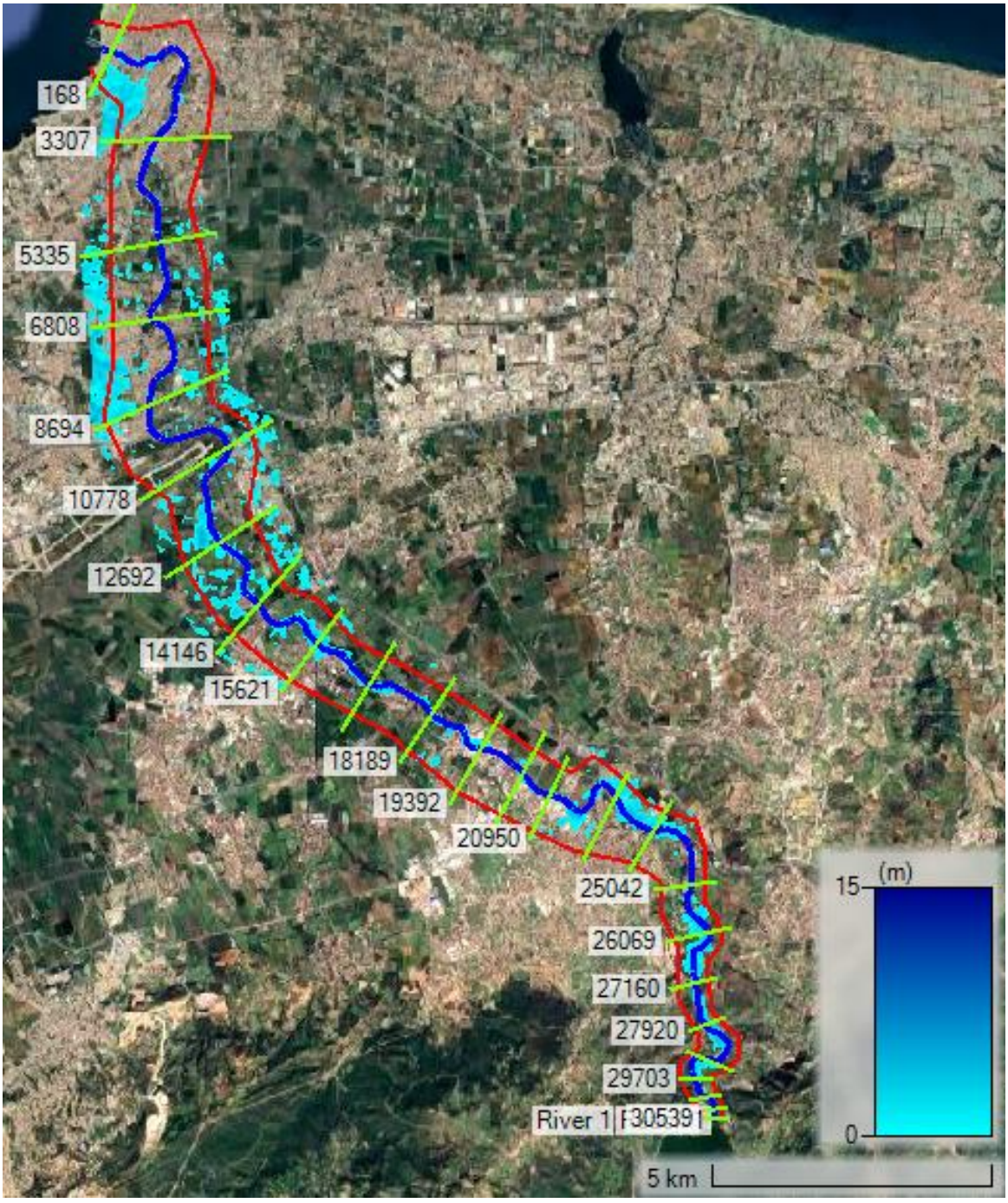

Fig 4.3: Map of the water depth

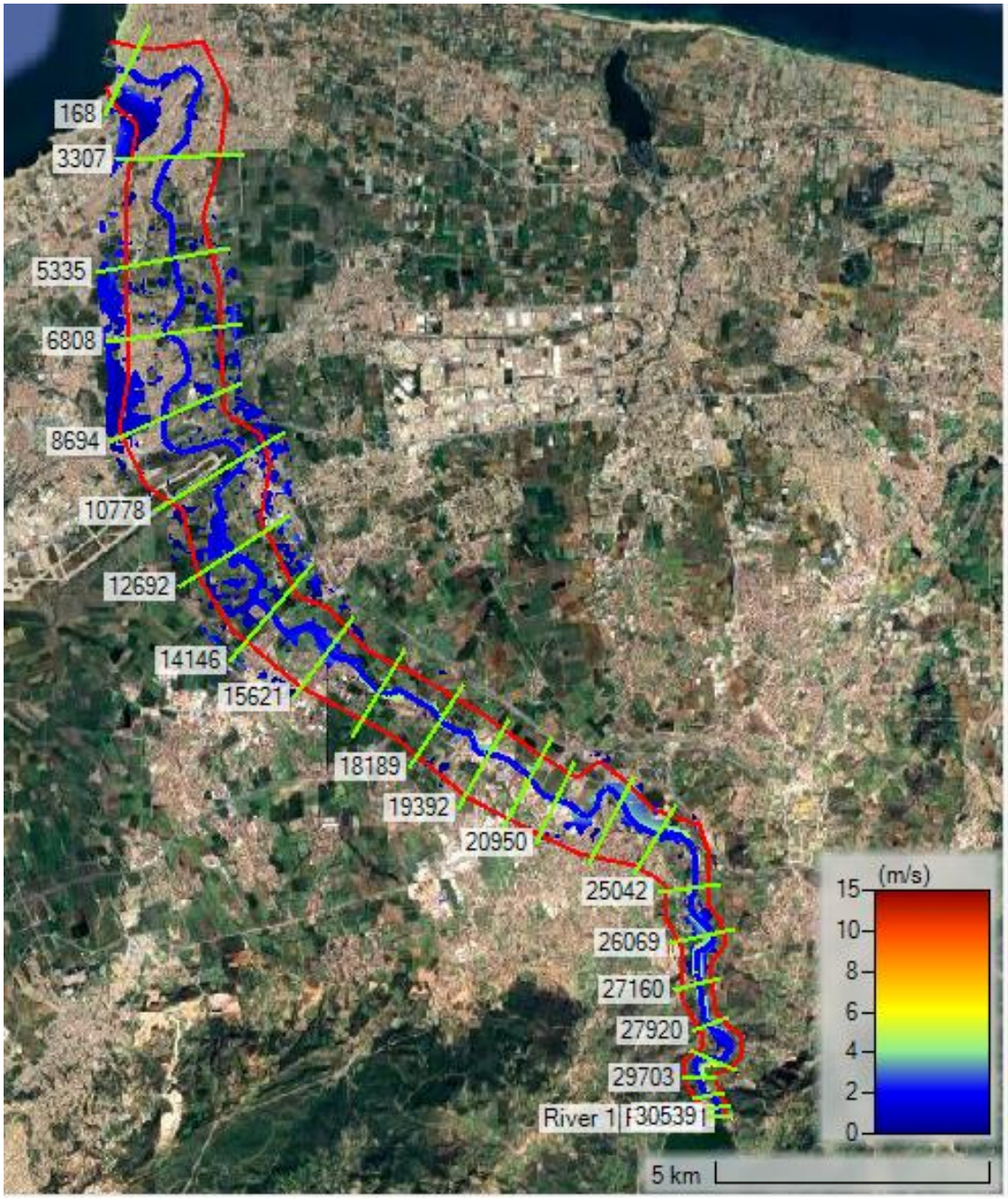

Fig 4.4: Map of velocity

4.8 Unsteady flow Simulation

As demonstrated by the steady-flow simulation results, the city of Bordj El Bahri faces the highest flood risk from Wadi El Hamiz. To enable a more accurate and detailed assessment, an unsteady-flow simulation of the region was conducted. The results of this simulation are presented below.

4.8.1 The water depth evolution

The unsteady-flow simulation enables generation of an animation depicting flood progression within the study area. It also facilitates production of flood maps at discrete time steps. The following section presents an analysis of flood evolution across these time intervals.

a. At t=2h

At this stage of the simulation, water levels are beginning to rise, mainly within the main channel. Flooding is still limited, and no significant overbank flow is observed yet.

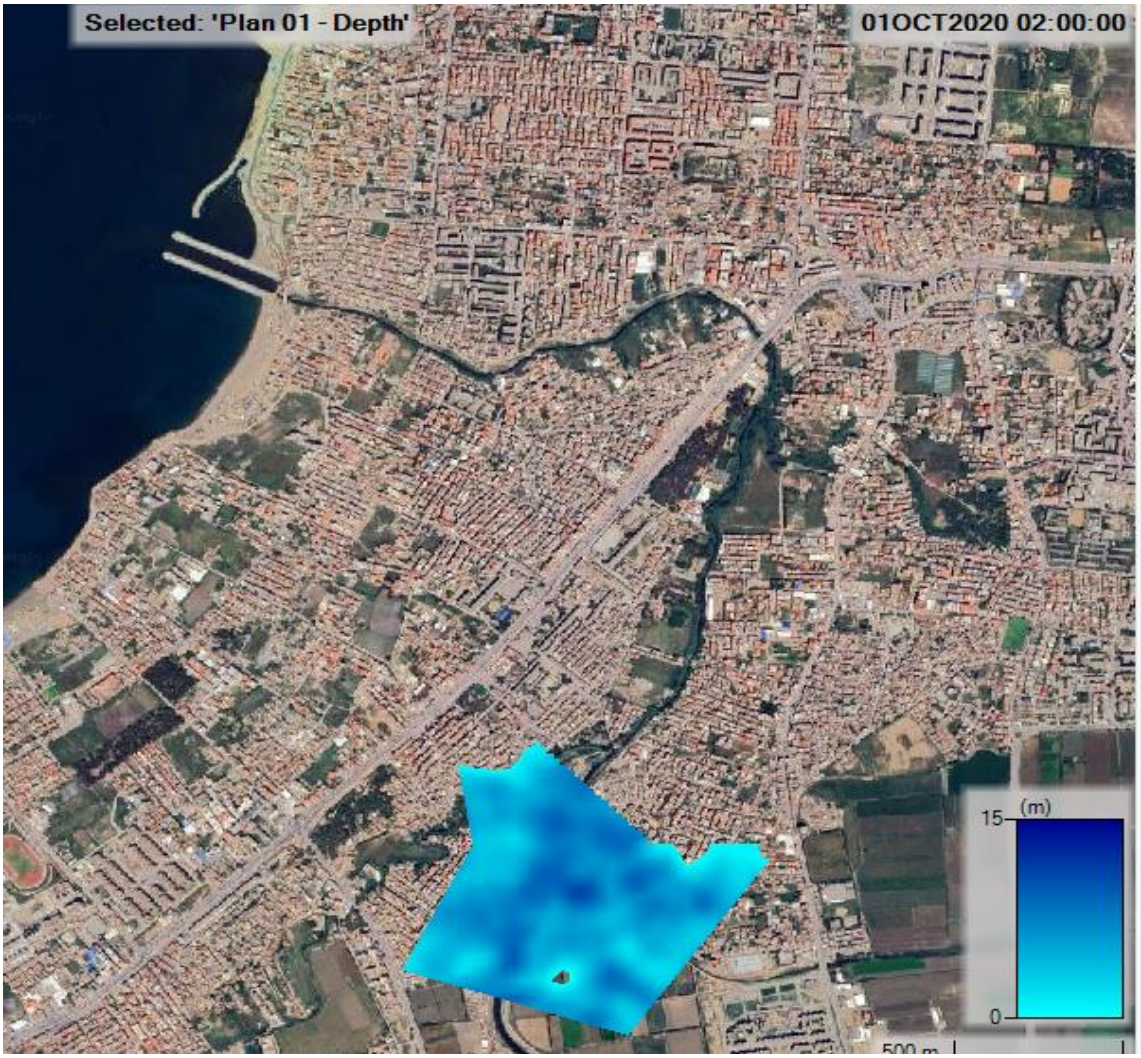

Fig 4.5: Water depth map at t=2h

a. At t=3h

By the third hour, the flood wave has advanced noticeably. Water starts to extend beyond the banks, especially in lower elevation areas, indicating the early stages of inundation in flood-prone zones.

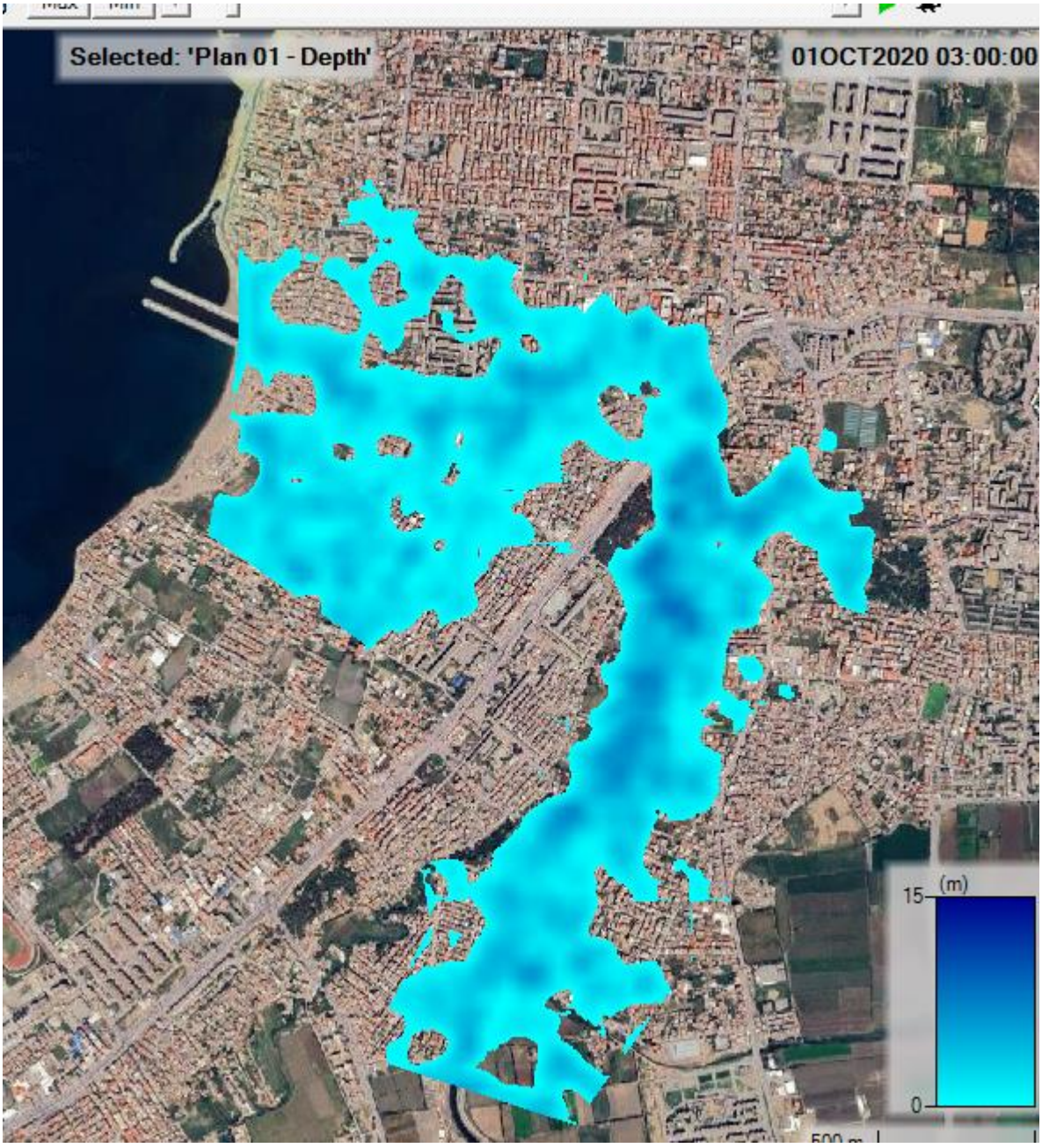

Fig 4.6: Water depth map at t=3h

a. At t=4 h

This marks the peak of the flood. Maximum water depths are recorded here, with large portions of the surrounding land submerged, confirming that this is the critical time for flood extent and emergency response planning.

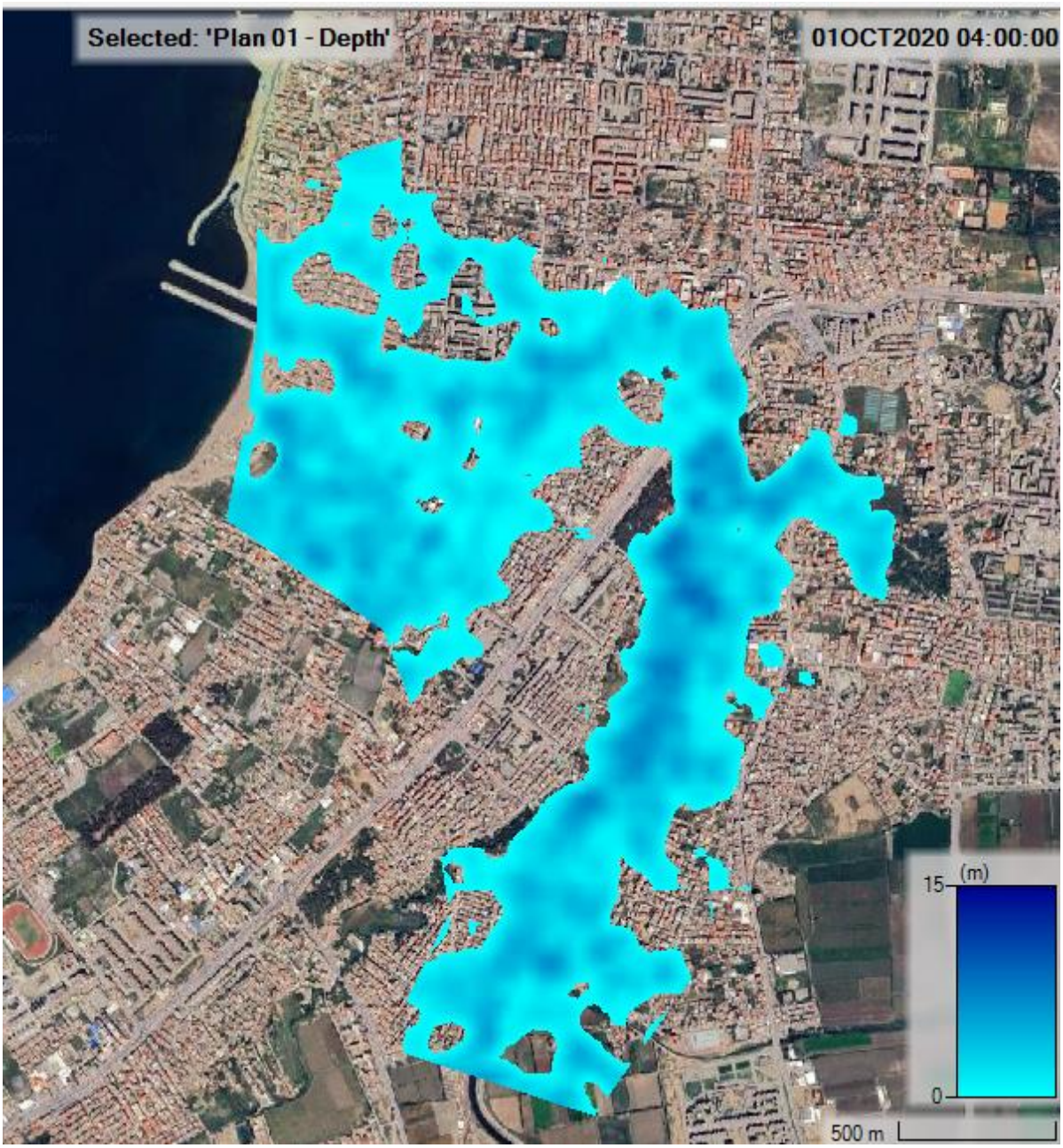

Fig 4.7: Water depth map at t=2h

a. At t=16h

At 16 hours, the flood has largely receded from its peak. However, some zones remain flooded, particularly those with poor drainage or flat topography, highlighting the importance of evaluating water retention areas.

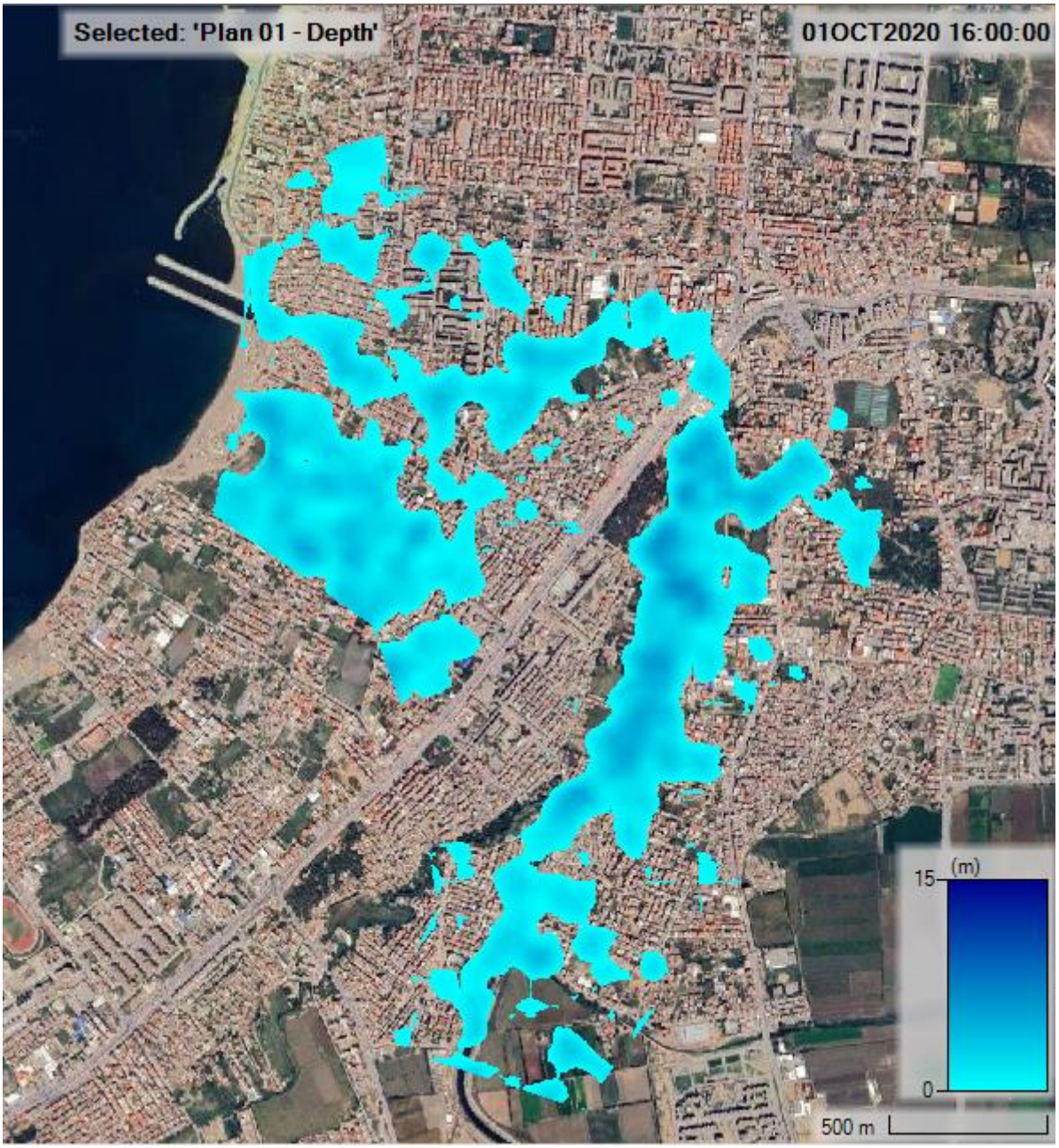

Fig 4.8: Water depth map at t=2h

a. At t=36 h

By the end of the simulation, most of the water has drained back into the channel or downstream. Only minimal residual flooding remains, emphasizing natural retention and slow drainage dynamics in certain zones.

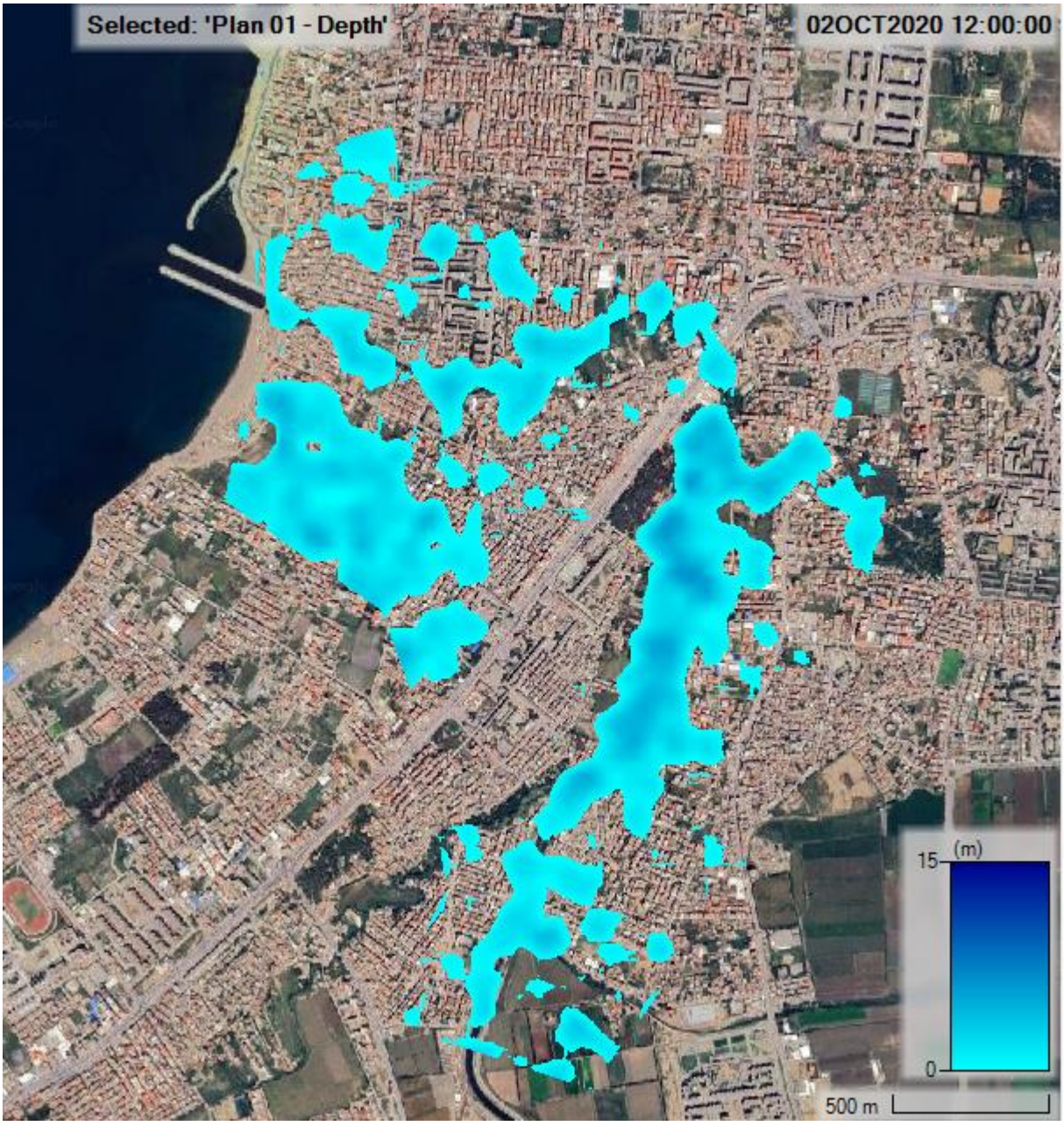

Fig 4.9: Water depth map at t=2h

4.8.1.1 Max water surface

This map represents the cumulative extent of flooding throughout the event. It clearly identifies all zones affected by the peak water levels and serves as a basis for flood hazard mapping and risk assessment.

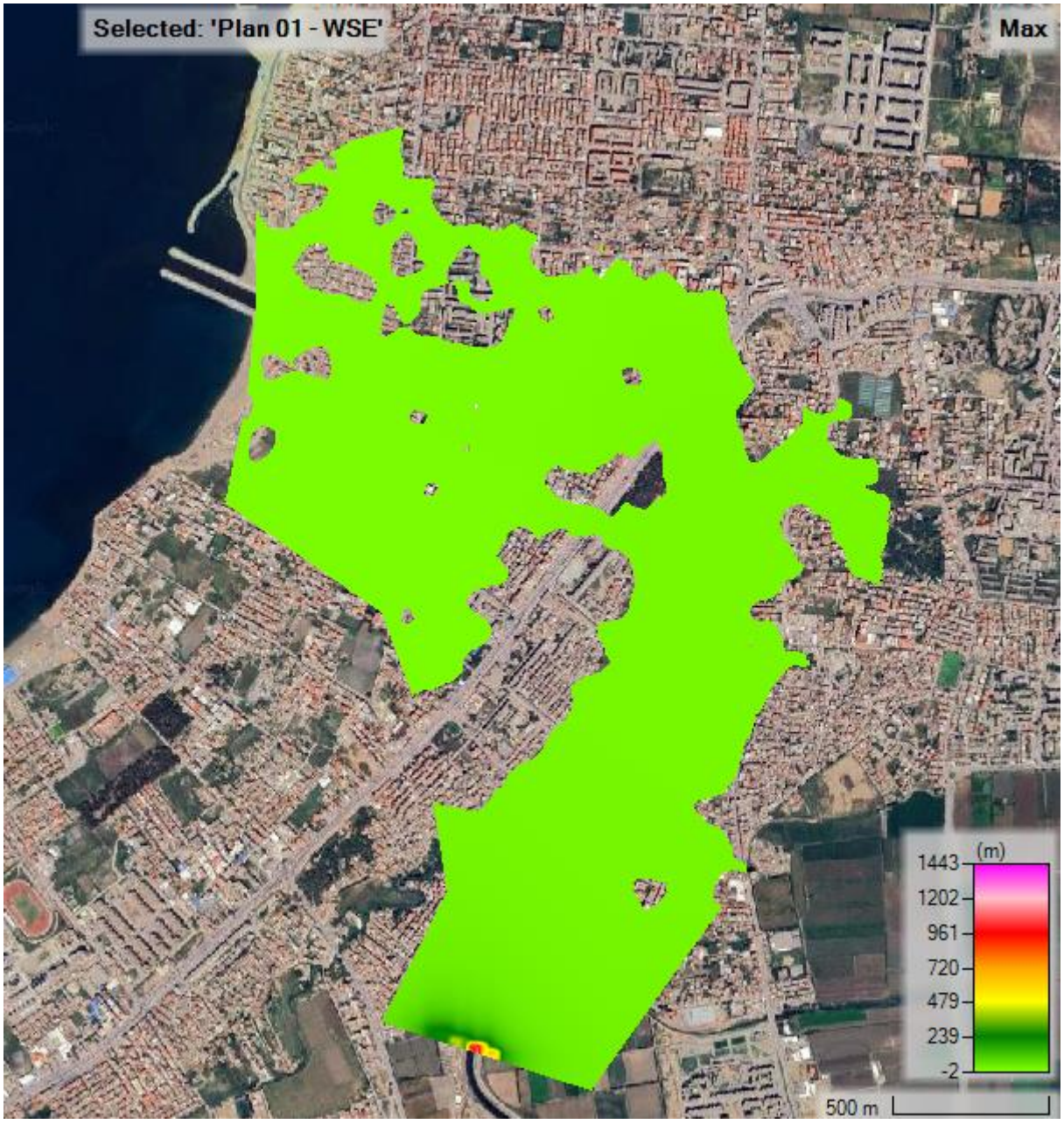

Fig 4.10: max water extent

4.8.1.2 Velocity analysis

High flow velocities are observed near the main riverbed, particularly during the flood peak. These areas could pose erosion risks or structural damage, especially where flow exceeds safe velocity thresholds.

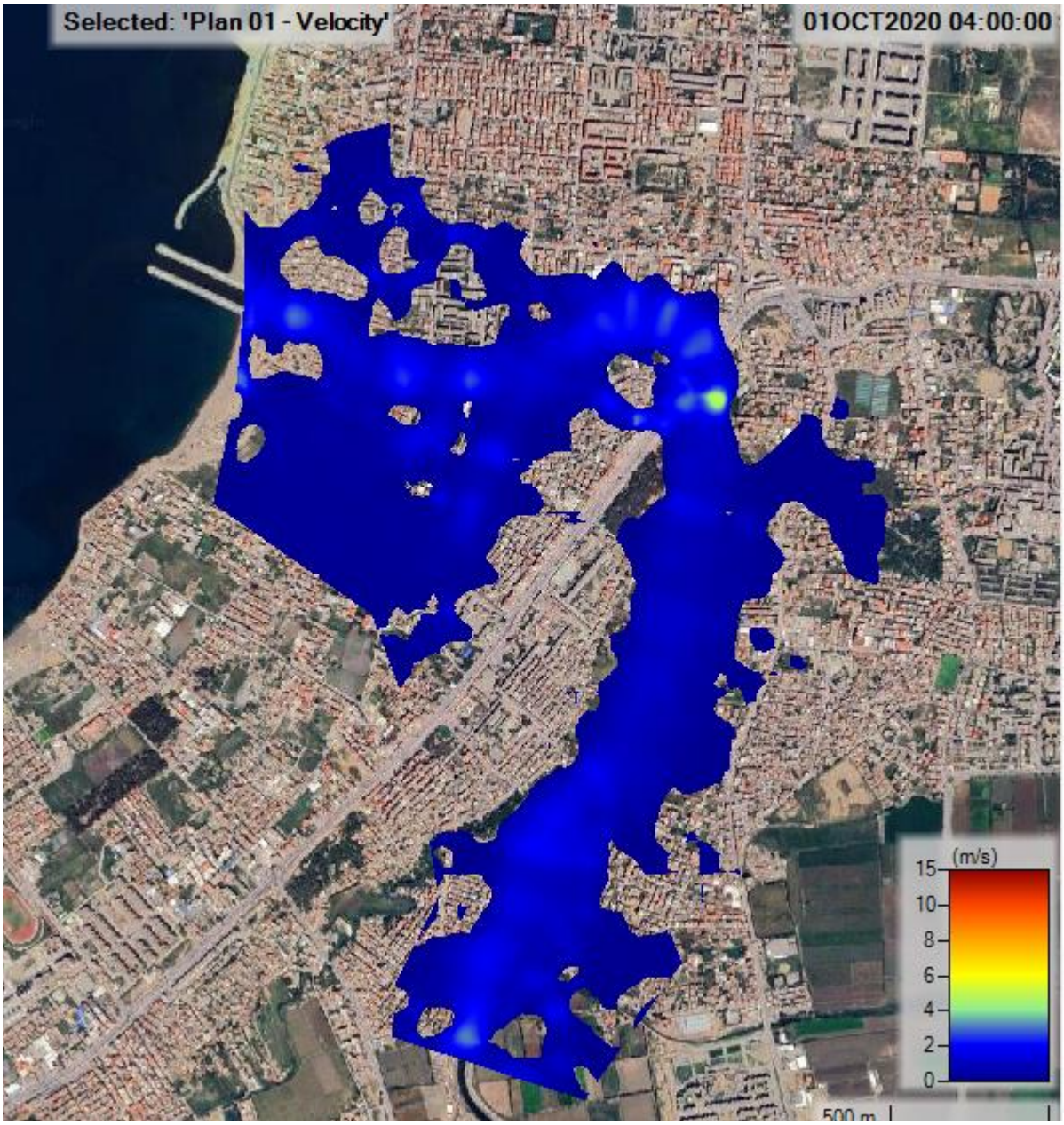

Fig 4.11: Map velocity at t=4h

4.9 Profile lines analysis

The profile lines define longitudinal sections (**see Annex-B- figures**) used to track water surface changes over time. They allow for detailed temporal analysis of the flood wave as it progresses through the system.

Fig 4.12: profile lines location

4.9.1 Profile 1 analysis

Profile 1 provides a clear visualization of the temporal evolution of the water surface at a specific cross section along the Bordj El Bahri reach. As shown in the time series (**figure 4.13**), there is a rapid increase in water level between the 2nd and 4th hour**,** indicating the arrival of the flood peak. This sharp rise reflects the dynamic nature of the flood wave, which corresponds with the previously identified peak flow time in the unsteady simulation.

The maximum water level is reached around t = 4h**,** after which the curve begins to decline gradually. This behavior is consistent with a flash-flood response typically observed in semi-urban basins with moderate to low storage capacity. The post-peak recession phase is more gradual, suggesting a relatively slow drainage process, possibly due to flat terrain downstream or lack of efficient drainage infrastructure.

This profile highlights the importance of early flood detection**,** as the short time between the initial rise and the peak leaves a narrow window for intervention. Moreover, if this location corresponds to a vulnerable urban or infrastructural area, it would be essential to consider mitigation strategies such as improved drainage design, retention structures, or flood barriers.

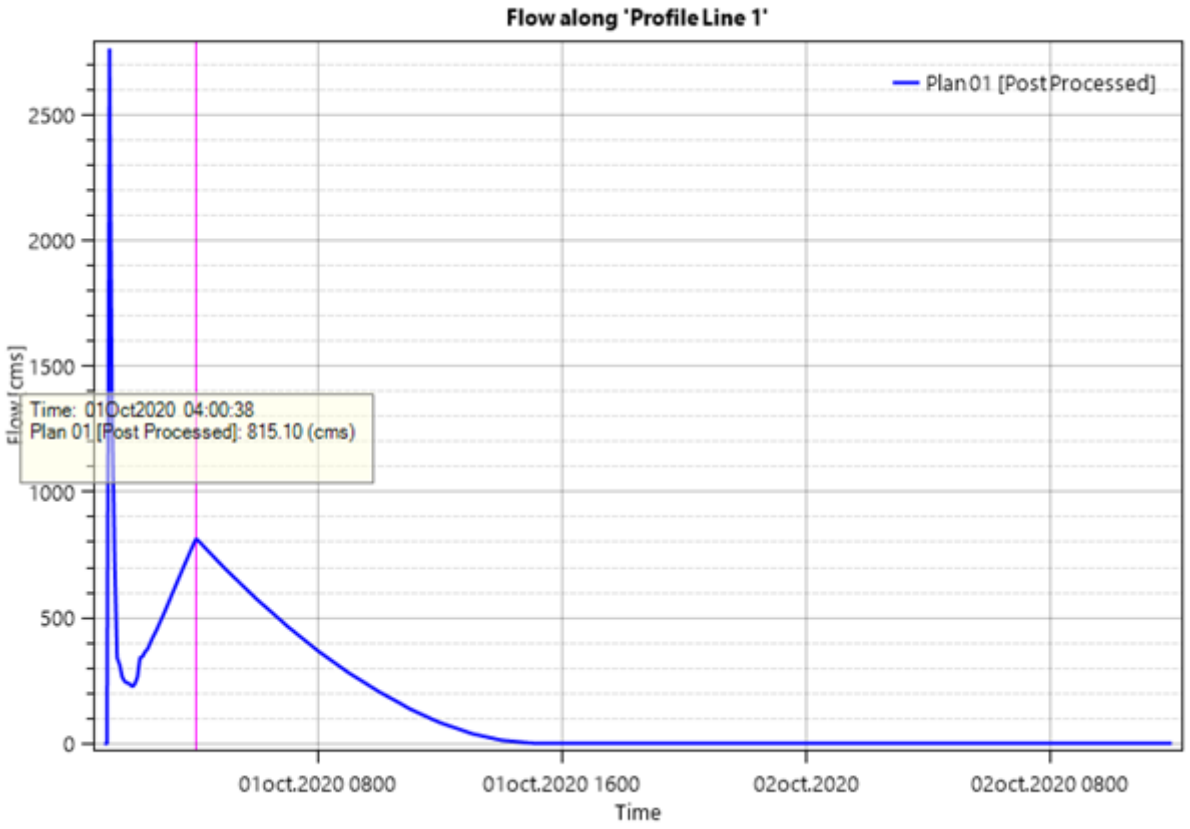

Fig 4.13 : Profile 1 time series.

4.9.2 Profile 2 analysis :

The water surface time series at Profile 2 reveals a flood behavior pattern similar to that observed in Profile 1, with a **steep rise in water level beginning shortly after the 2nd hour**. The hydrograph reaches its **maximum height at approximately 4 hours**, confirming that this section also experienced the flood peak during the same critical time window. The synchronicity of the peak across profiles suggests a **coherent and fast-moving flood wave** throughout the river reach.

Following the peak, the water level at Profile 2 declines gradually, indicating a slower withdrawal of water. This may be attributed to low channel slope, mild topography, or downstream flow restrictions that reduce the recession rate. Given the magnitude and duration of inundation at this point, Profile 2 represents a location where sustained flooding could **occur**,

emphasizing the need for floodplain zoning and possibly controlled overflow areas to reduce downstream impacts.

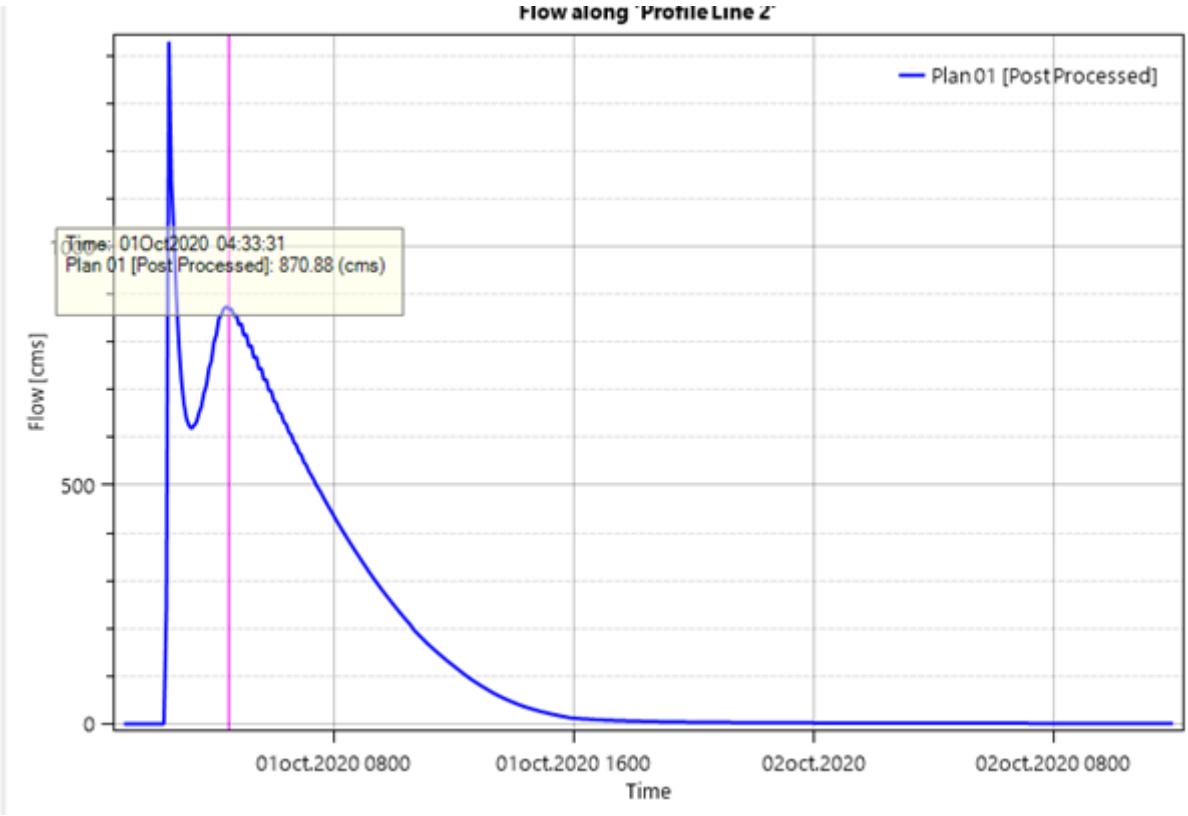

Fig 4.14 : Profile 2 time series.

4.9.3 Profile 3 analysis :

Profile 3 displays a slightly **delayed but still distinct flood response**, with the water level rising rapidly and peaking around the **4th hour**, similar to the other profiles. The hydrograph shape is slightly more rounded, suggesting that **this location may be influenced by local storage effects**, channel widening, or reduced flow velocity.

Despite this, the peak water level remains significant, and the **extended recession period** indicates that water tends to linger in this are**a**, likely due to flat terrain or insufficient drainage capacity. Such behavior increases the risk of prolonged inundation, particularly if the area includes urban development or agricultural land. From a flood risk management perspective, Profile 3 underlines the importance of integrating land-use planning with hydraulic modeling outputs to identify zones prone not only to peak flooding but also to delayed water re**cession**.

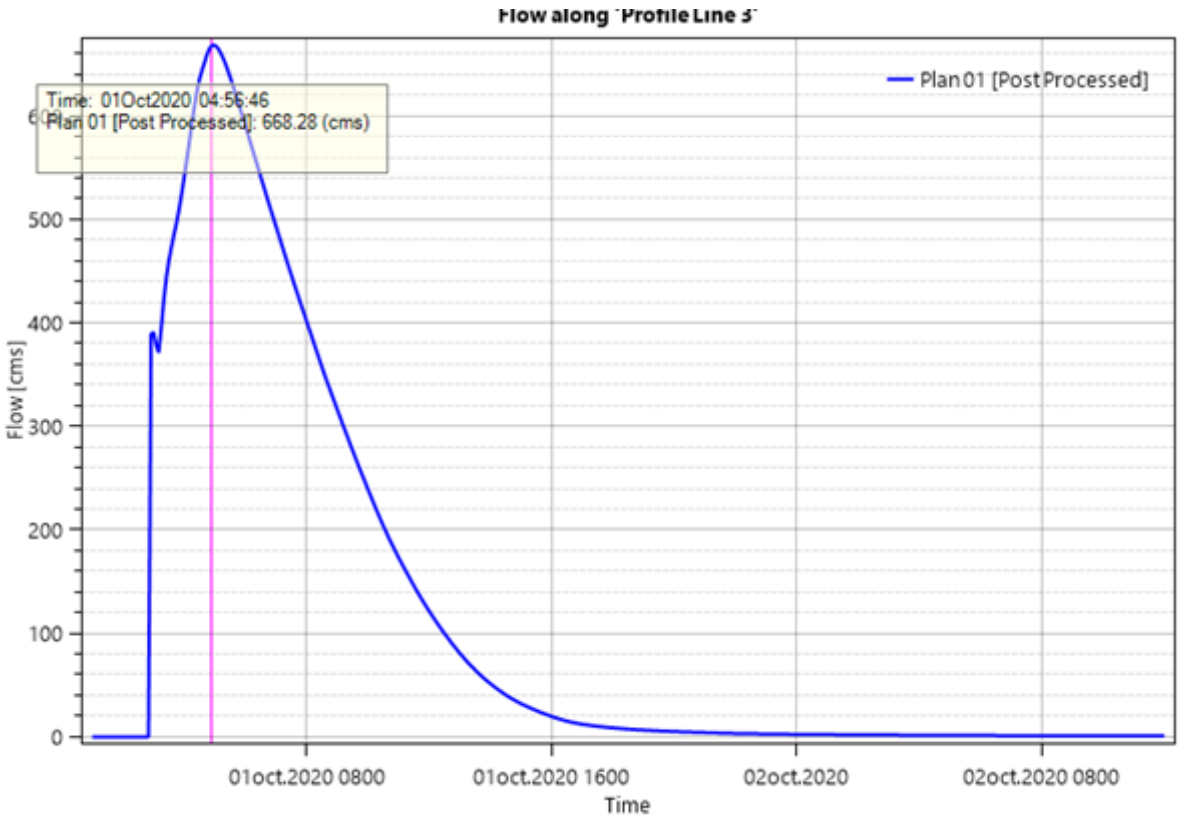

Fig 4.15 : Profile 3 time series.

4.10 Conclusion

This chapter has established a comprehensive hydraulic modeling framework for flood risk assessment in the El Hamiz watershed using HEC-RAS simulations. Through rigorous evaluation of seven empirical methods, a conservative peak discharge of 948.12 m^3/s (100-year return period) was determined, incorporating the Mallet-Gauthier formula's worst-case scenario and spillway capacity. Coupled with a critical time of concentration (Tc = 3.83 h) derived via the Ventura formula, these parameters informed a Sokolovsky synthetic hydrograph to drive both steady and unsteady flow simulations. Steady-state results identified four high-risk inundation zones: Ben Ammar's residential areas, Houari Boumediene Airport's eastern runway, El Hamiz city along National Road 5, and Bordj El Bahri—with flooding severity strongly correlated to topographic flatness and reduced flow velocities attributable to gentle channel slopes. Unsteady simulation revealed critical temporal dynamics: rapid floodwave propagation peaked at t=4h, with maximum depths exceeding 3.5 m in urbanized Bordj El Bahri, followed by prolonged recession (>36 hours) in topographically constrained areas. Longitudinal profile analyses confirmed synchronized flood progression across the watershed, while highlighting delayed drainage in downstream reaches due to minimal slope. These findings underscore Bordj El Bahri's acute vulnerability given its dense population, maximum

flood extent, and Mediterranean exposure. The analysis provides foundational data for evidence-based mitigation strategies—prioritizing zones where land-use planning, structural interventions, and emergency response protocols require urgent enhancement to address escalating flood risks in Algiers' rapidly urbanizing periphery.

GENERAL CONCLUSION

General Conclusion

This study has contributed to a better understanding of flood dynamics within the studied watershed through the application of numerical simulation using the HEC-RAS software. The results obtained clearly identified the areas most vulnerable to flooding, as well as the expected water surface elevations and flow velocities under various flood scenarios. These findings highlight the exposure of certain zones to significant flood hazards and emphasize the necessity for careful land-use planning and risk mitigation strategies.

The use of HEC-RAS proved to be particularly valuable for modeling riverine flows and simulating flood behavior. Its ability to handle both steady and unsteady flow conditions allowed for detailed analysis of hydraulic phenomena and provided a reliable representation of flood extents. As such, this method serves as an effective decision-support tool for planners, engineers, and policymakers involved in flood risk management and territorial development.

Nevertheless, the study faced several limitations. The accuracy of the simulation heavily depends on the quality and resolution of input data, particularly topographic and hydrological datasets. Additionally, some critical variables such as land-use change, soil infiltration capacity, and climate variability could not be fully integrated into the model. The simulation also does not fully capture the complexity of human-environment interactions, which play a significant role during actual flood events.

Looking forward, several perspectives can be considered to enhance the scope and reliability of such studies. Integrating more detailed rainfall and climate projections would allow for better evaluation of future flood risks under changing conditions. Coupling HEC-RAS with other hydrological and GIS-based tools could lead to more comprehensive analyses. Furthermore, the development of local flood management plans, early warning systems, and public awareness initiatives would be key steps toward building community resilience and improving preparedness for flood events.

BIBLIOGRAPHY

Bibliographic references

Abbott, M. B., & Minns, A. W. (1998). Computational Hydraulics. Routledge.

Alexander, D. (1993). Natural Disasters. Chapman & Hall.

Alamri, N., Afolabi, K., Ewea, H., & Elfeki, A. (2023). Evaluation of the time of concentration models for enhanced peak flood estimation in arid regions. Sustainability, 15(3), 1987.

Anderson, J. D. (1995). Computational Fluid Dynamics: The Basics with Applications. McGraw-Hill.

Baran-Zgłobicka, B., Godziszewska, D., & Zgłobicki, W. (2021). The flash floods risk in the local spatial planning (case study: Lublin Upland, E Poland). Resources, 10(2), 14.

Bates, P. D., & De Roo, A. (2000). A simple raster-based model for flood inundation simulation. Journal of Hydrology, 236(1–2), 54–77.

Bouach, A. (2011). Numerical Simulation of Solid Transport by Bed-Load Using the RUBAR20TS Computation Code (Magister's thesis). École Nationale Polytechnique. 149 p.

Brunner, G. W. (2020). HEC-RAS River Analysis System – User's Manual, Version 6.0. U.S. Army Corps of Engineers, HEC.

Chu, S. T., & Shirmohammadi, A. (2004). "Comparison of SCS Unit Hydrograph and Kinematic Wave Models for Runoff Simulation." Hydrological Processes, 18(3), 563–575.

Coppola, A. I., Todini, E., & Versace, P. (2017). Hydrological analysis of concentration time formulas in Mediterranean basins. Journal of Hydrology and Hydromechanics, 65(4), 367–375.

Cunge, J. A., Holly, F. M., & Verwey, A. (1980). Practical Aspects of Computational River Hydraulics. Pitman Publishing.

De Michele, C., & Salvadori, G. (2002). Hydrological analysis using empirical concentration time formulas in ungauged Mediterranean basins. Hydrology and Earth System Sciences, 6(1), 41–48.

Di Baldassarre, G., et al. (2010). Flood fatalities in Africa: From diagnosis to mitigation. Geophysical Research Letters, 37(22).

Few, R., Ahern, M., Matthies, F., & Kovats, S. (2004). Floods, health and climate change: A strategic review. Tyndall Centre for Climate Change Research.

Gartsman, B. I. (2008). Time of concentration estimation in small mountainous watersheds. Journal of Hydrology and Hydromechanics, 56(3), 189–198.

Guha-Sapir, D., Hoyois, P., & Below, R. (2017). Annual Disaster Statistical Review 2016: The Numbers and Trends. CRED.

Hirabayashi, Y., et al. (2013). Global flood risk under climate change. Nature Climate Change, 3(9), 816–821.

Horritt, M. S., & Bates, P. D. (2002). Evaluation of 1D and 2D numerical models for predicting river flood inundation. Journal of Hydrology, 268(1–4), 87–99.

IPCC (Intergovernmental Panel on Climate Change). (2014). Climate Change 2014: Impacts, Adaptation, and Vulnerability. Cambridge University Press.

Jonkman, S. N. (2005). Global perspectives on loss of human life caused by floods. Natural Hazards, 34(2), 151–175.

Kundzewicz, Z. W., & Takeuchi, K. (1999). Flood protection and management: Quo vadimus? Hydrological Sciences Journal, 44(3), 417–432.

Liggett, J. A., & Cunge, J. A. (1975). Numerical Methods of Solution of the Unsteady Flow Equations. In Unsteady Flow in Open Channels (Vol. 1). Water Resources Publications.

Mardaid, E., Abidin, Z. Z., Asmai, S. A., & Abas, Z. A. (2023). Implementation of Flood Emergency Response System with Face Analytics. International Journal of Advanced Computer Science and Applications, 14(1).

Mishra, S. K., & Singh, V. P. (2003). Soil Conservation Service Curve Number (SCS-CN) Methodology. Springer.

Mockus, V. (1964). Hydrology. National Engineering Handbook, Section 4. USDA-SCS.

National Oceanic and Atmospheric Administration. (2023). National Coastal Flood Risk Assessment [Report]. https://www.noaa.gov/jetstream/2004tsu_max

Noji, E. K. (2005). Public health in the aftermath of disasters. BMJ, 330(7504), 1379–1381.

Parker, D. J. (2000). Floods. Routledge.

Pappenberger, F., Beven, K. J., Hunter, N. M., Bates, P. D., Gouweleeuw, B. T., Thielen, J., & De Roo, A. (2005). Cascading model uncertainty from medium range weather

forecasts through a rainfall–runoff model to flood inundation predictions. Hydrology and Earth System Sciences, 9(4), 381–393.

Pinder, G. F., & Gray, W. G. (1977). Finite Element Simulation in Surface and Subsurface Hydrology. Academic Press.

Remini, B., & Achour, B. (2009). Analyse comparative des formules empiriques du temps de concentration pour les bassins méditerranéens. Revue des Sciences de l'Eau, 22(3), 275–286.

Saint-Venant, A. J. C. B. (1871). Théorie du mouvement non permanent des eaux, avec application aux crues des rivières et à l'introduction des marées dans leur lit. Comptes Rendus de l'Académie des Sciences, 73, 147–154.

Singh, V. P. (1996). Kinematic Wave Modeling in Water Resources: Surface-Water Hydrology. Wiley.

Sokolovsky, D. S. (1968). Hydrological Basis of Surface Water Modeling. Moscow: Hydrometeoizdat.

Todorovic, P., & Maksimovic, C. (1987). Empirical formulas for estimating time of concentration in Eastern European catchments. Journal of Hydrology, 92(3–4), 299–310.

U.S. Army Corps of Engineers (USACE). (2020). HEC-RAS Overview and Applications. Hydrologic Engineering Center.

UNISDR (United Nations Office for Disaster Risk Reduction). (2015). Sendai Framework for Disaster Risk Reduction 2015–2030.

Versace, P., Ferrari, E., & Iovino, F. (2001). Idrologia e Modellistica Idrologica. McGraw-Hill, Milano.

Ward, P. J., et al. (2013). Assessing flood risk at the global scale: Model setup, results, and sensitivity. Environmental Research Letters, 8(4), 044019.

WHO (World Health Organization). (2013). Floods: Climate change and adaptation strategies for human health.

Zhang, H., Qi, Z., Li, X., Chen, Y., Wang, X., & He, Y. (2021). An urban flooding index for unsupervised inundated urban area detection using Sentinel-1 polarimetric SAR images. Remote Sensing, 13(22), 4511.

Bibliographic references

Alfieri, L., Burek, P., Feyen, L., & Forzieri, G. (2015). Global warming increases the frequency of river floods in Europe. Hydrology and Earth System Sciences, 19, 2247–2260. https://doi.org/10.5194/hess-19-2247-2015

Brunner, G. W. (2020). HEC-RAS River Analysis System User's Manual Version 6.0. U.S. Army Corps of Engineers, Hydrologic Engineering Center.

Horritt, M. S., & Bates, P. D. (2002). Evaluation of 1D and 2D numerical models for predicting river flood inundation. Journal of Hydrology, 268(1–4), 87–99. https://doi.org/10.1016/S0022-1694(02)00121-X

IPCC (2022). Climate Change 2022: Impacts, Adaptation and Vulnerability. Contribution of Working Group II to the Sixth Assessment Report of the Intergovernmental Panel on Climate Change.

Kundzewicz, Z. W., et al. (2014). Flood risk and climate change: global and regional perspectives. Hydrological Sciences Journal, 59(1), 1–28. https://doi.org/10.1080/02626667.2013.857411

Teng, J., Vaze, J., Dutta, D., Marvanek, S., & Ticehurst, C. (2017). Flood inundation modelling: A review of methods, recent advances and uncertainty analysis. Environmental Modelling & Software, 90, 201–216. https://doi.org/10.1016/j.envsoft.2017.01.006

WEBOGRAPHY

Webography

ArcGIS Online – ESRI: https://www.arcgis.com/

Climate-Data.org – Algeria Climate Zones: https://en.climate-data.org/africa/algeria/

CNTS – Centre National des Technologies Spatiales (Algérie): http://www.cnts.dz/

Copernicus – European Space Agency (ESA): https://www.copernicus.eu/en

Google Earth: https://earth.google.com/

Google Scholar: https://scholar.google.com/

Global Flood Monitoring System (University of Maryland): https://flood.umd.edu/

Global Runoff Data Centre (GRDC): https://www.bafg.de/GRDC/

HydroSHEDS by WWF & USGS: https://www.hydrosheds.org/

Ministère des Ressources en Eau (Algérie): http://www.mre.gov.dz/

NASA Earthdata: https://earthdata.nasa.gov/

Office National de la Météorologie (Algérie): http://www.meteo.dz/

OpenStreetMap (OSM): https://www.openstreetmap.org/

ReliefWeb – Floods in Algeria: https://reliefweb.int/

ResearchGate: https://www.researchgate.net/

US Army Corps of Engineers – HEC-RAS Software: https://www.hec.usace.army.mil/software/hec-ras/

United Nations Environment Programme (UNEP): https://www.unep.org/

World Bank – Flood Risk Management: https://www.worldbank.org/en/topic/disasterriskmanagement

Annex –A-

Figure A1: The cross section 25042.

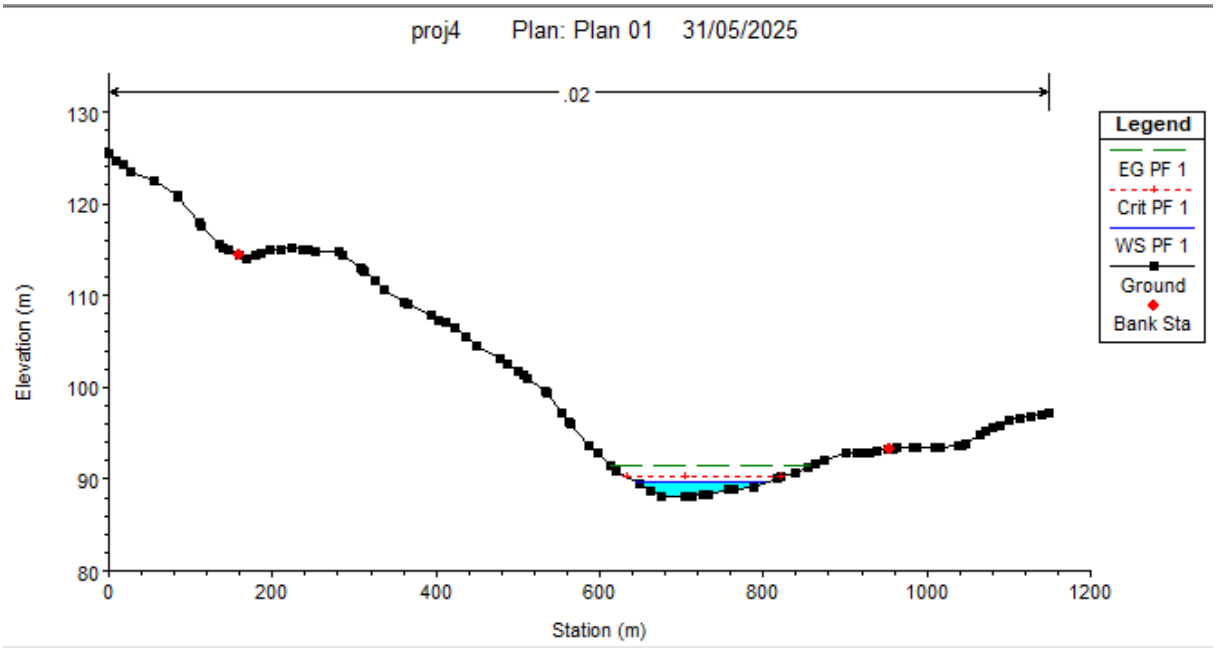

Figure A2: The cross section 15621

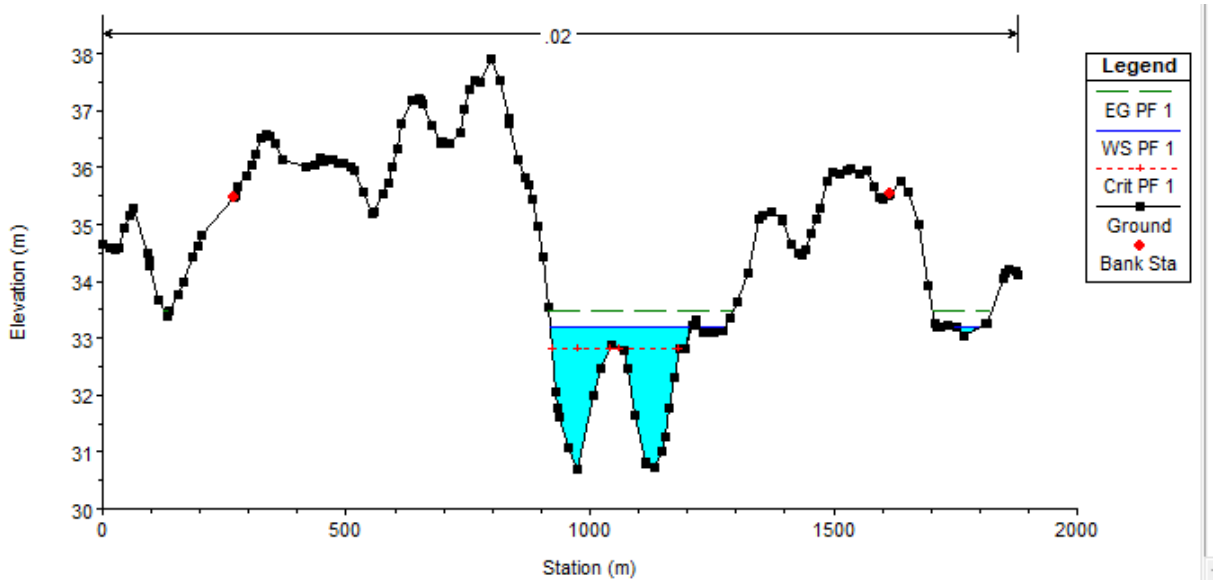

Figure A3: The cross section 10778

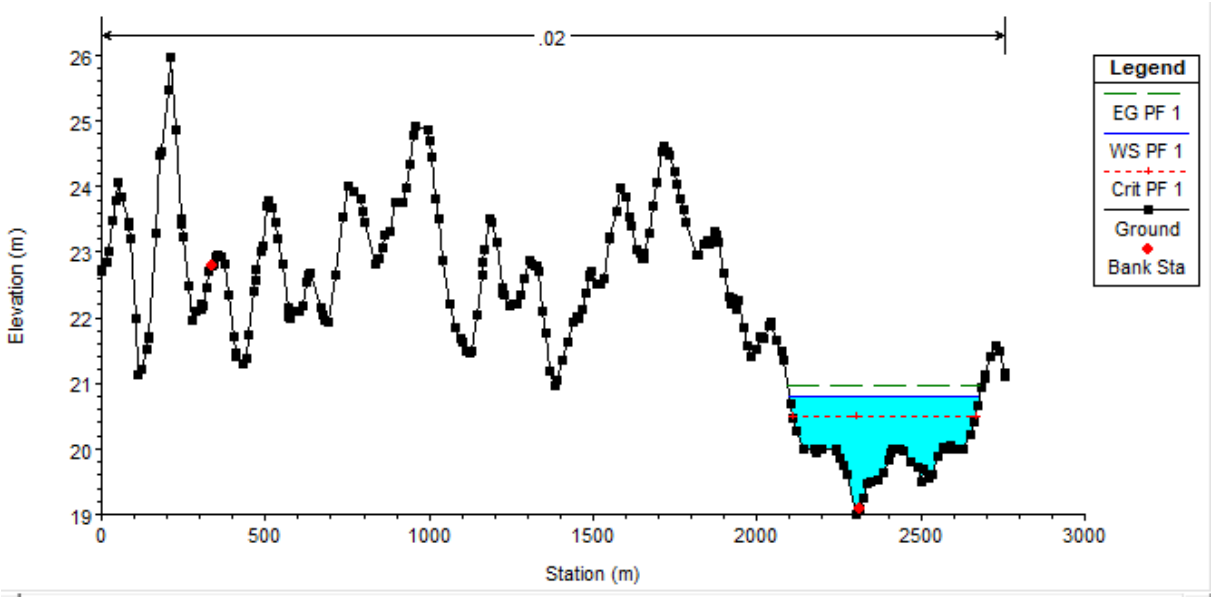

Figure A4: The cross section 8694

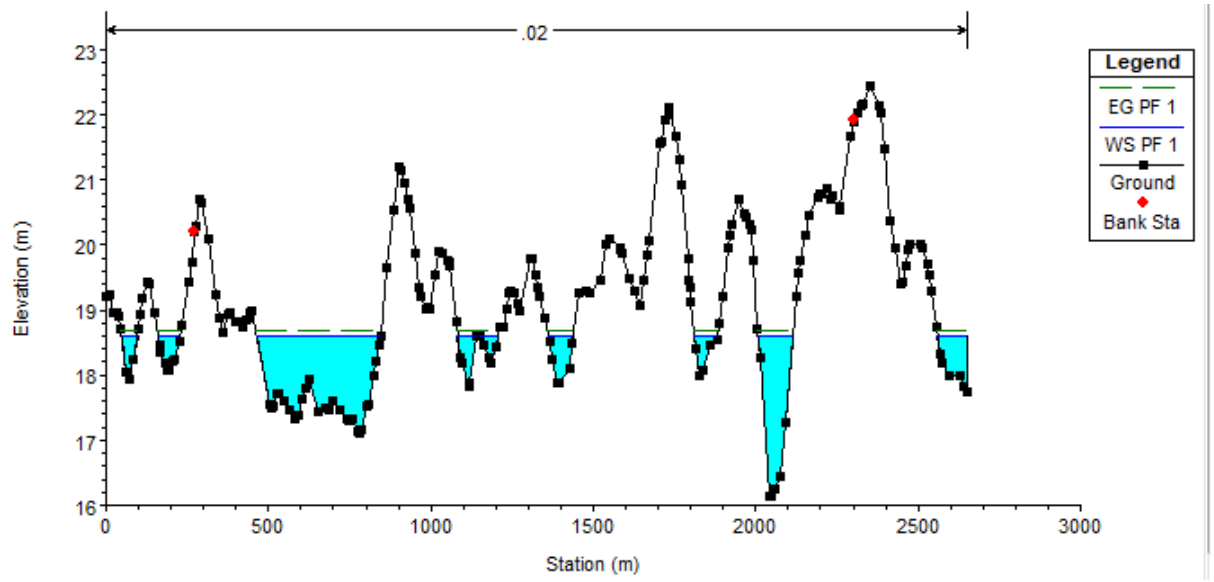

Figure A5: The cross section 3307

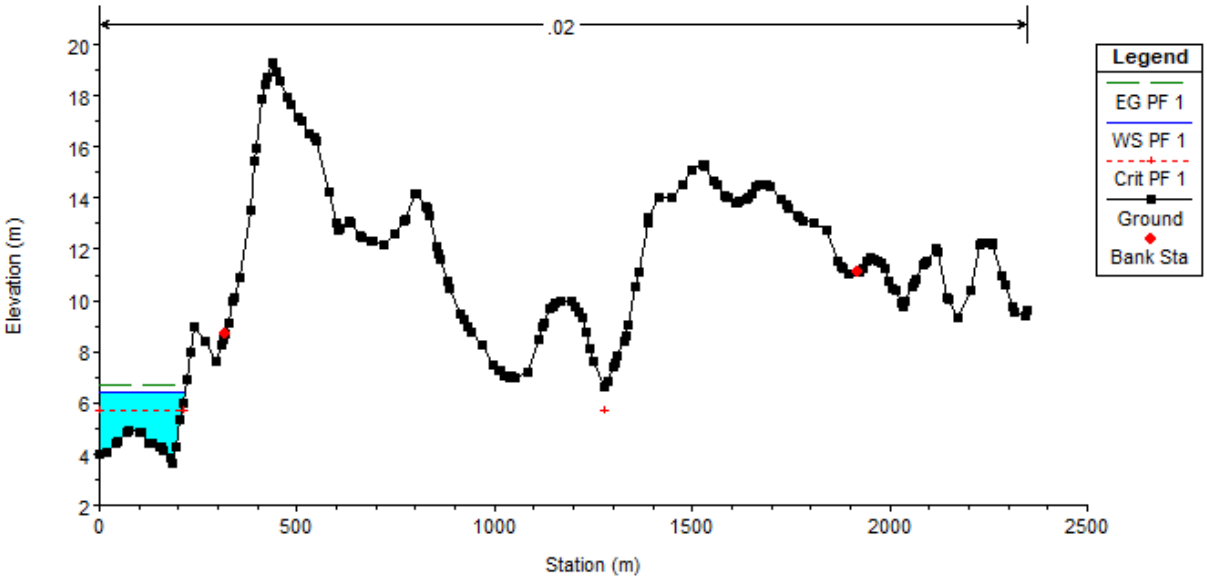

Figure A6: Profile view

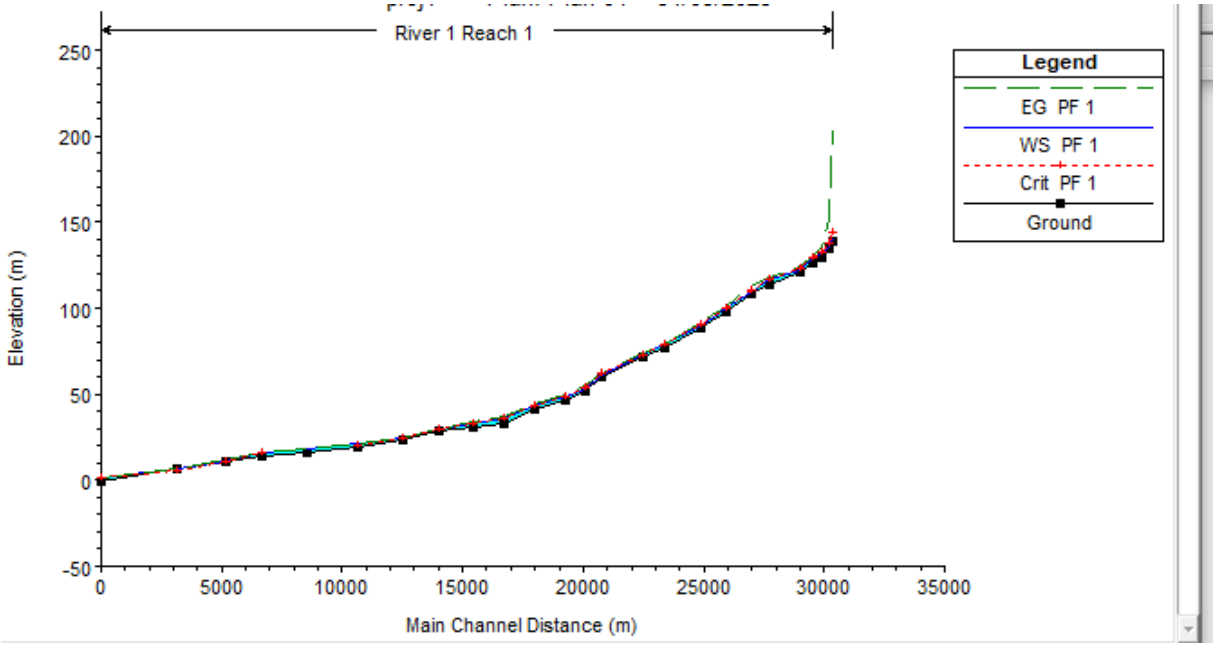

Annex

Table A1: Summary output

River Sta	Q Total (m3/s)	Min Ch El	W.S. Elev (m)	Crit W.S. (m)	E.G. Elev (m)	E.G. Slope (m/m)	Vel Chnl (m/s)	Flow Area (m2)	Top Width (m)	Froude
30539	948.1	138.74	140.64	143.84	203.78	0.500081	35.19	26.94	26.86	11.22
30381	948.1	134.84	136.12	137.98	151.38	0.140823	17.3	54.8	61.8	5.87
30095	948.1	129.1	131.12	132.28	135.25	0.021714	9.01	105.28	77.75	2.47
29703	948.1	126.31	129.3	129.57	130.4	0.005784	4.64	204.15	151.07	1.28
29140	948.1	120.52	122.13	122.83	124.46	0.023493	6.76	140.26	169.27	2.37
27920	948.1	113.96	116.84	116.85	117.65	0.003425	3.97	238.6	150.6	1.01
27160	948.1	108.24	109.74	110.44	112.13	0.022896	6.85	138.31	160.32	2.36
26069	948.1	98.01	100.06	100.21	100.68	0.00558	3.48	272.12	301.92	1.17
25042	948.1	88.02	89.59	90.18	91.52	0.015856	6.16	153.8	158.7	2
23571	948.1	76.49	78.7	78.77	79.3	0.004847	3.41	278.33	287.37	1.11
22636	948.1	71.71	73.05	73.23	73.72	0.007491	3.33	265.31	360.39	1.29
20950	948.1	59.64	61.66	61.89	62.48	0.005961	4.13	246.65	279.29	1.25
20286	948.1	51.39	52.95	53.6	55.25	0.024241	6.71	141.24	176.27	2.39
19392	948.1	46.01	48.88	48.88	49.56	0.00363	3.63	261.36	197.69	1.01
18189	948.1	41.03	43.41	43.61	44.41	0.005031	4.45	213.23	151.79	1.2
16870	948.1	33.38	35.98	36.33	37.36	0.005645	5.19	182.51	112.09	1.3
15621	948.1	30.68	33.19	32.81	33.49	0.001936	2.41	395.89	392.67	0.72
14146	948.1	28.39	29.34	29.34	29.67	0.003629	1.71	393.91	601.11	0.83

12692	948.1	23	24.03	24.11	24.47	0.003508	1.66	356.64	533.39	0.82
10778	948.1	19	20.81	20.49	20.96	0.001251	1.66	553.56	581.27	0.56

Annex –B-

Figure B1: Profile line 1.

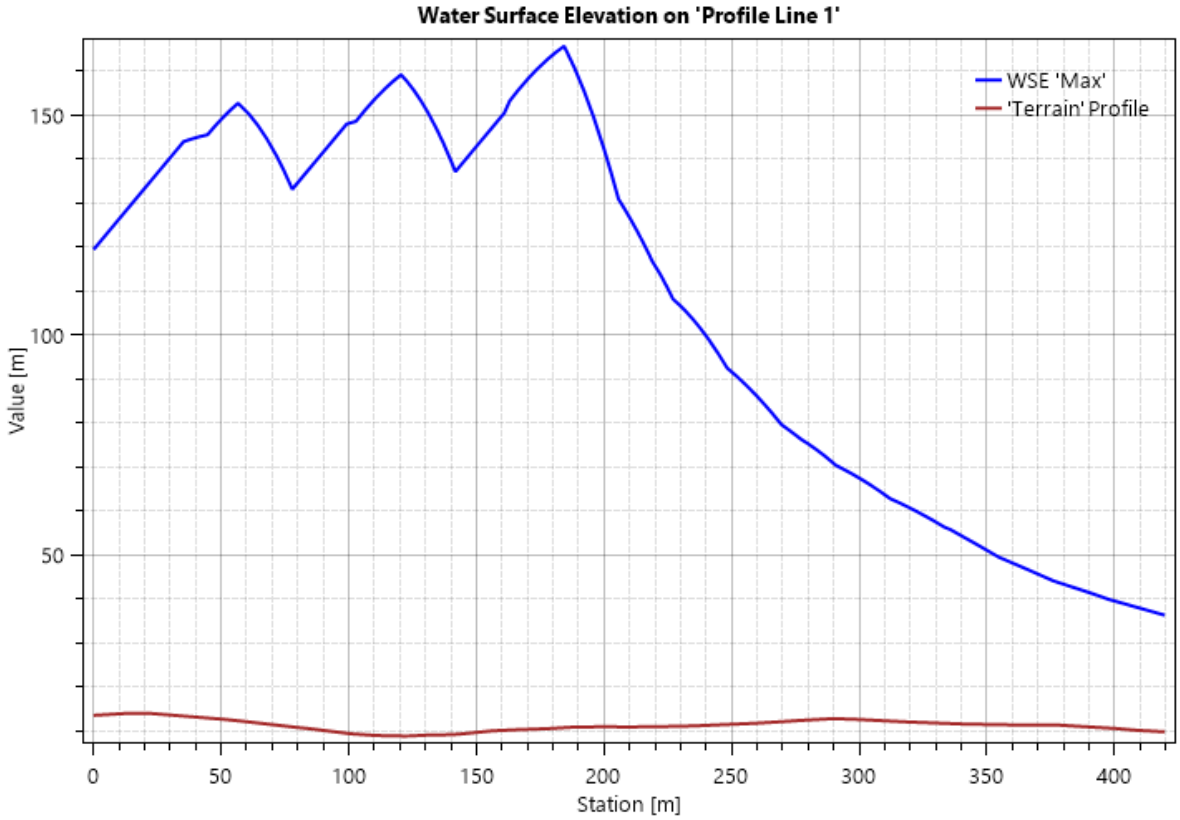

Figure B2: Profile line 2.

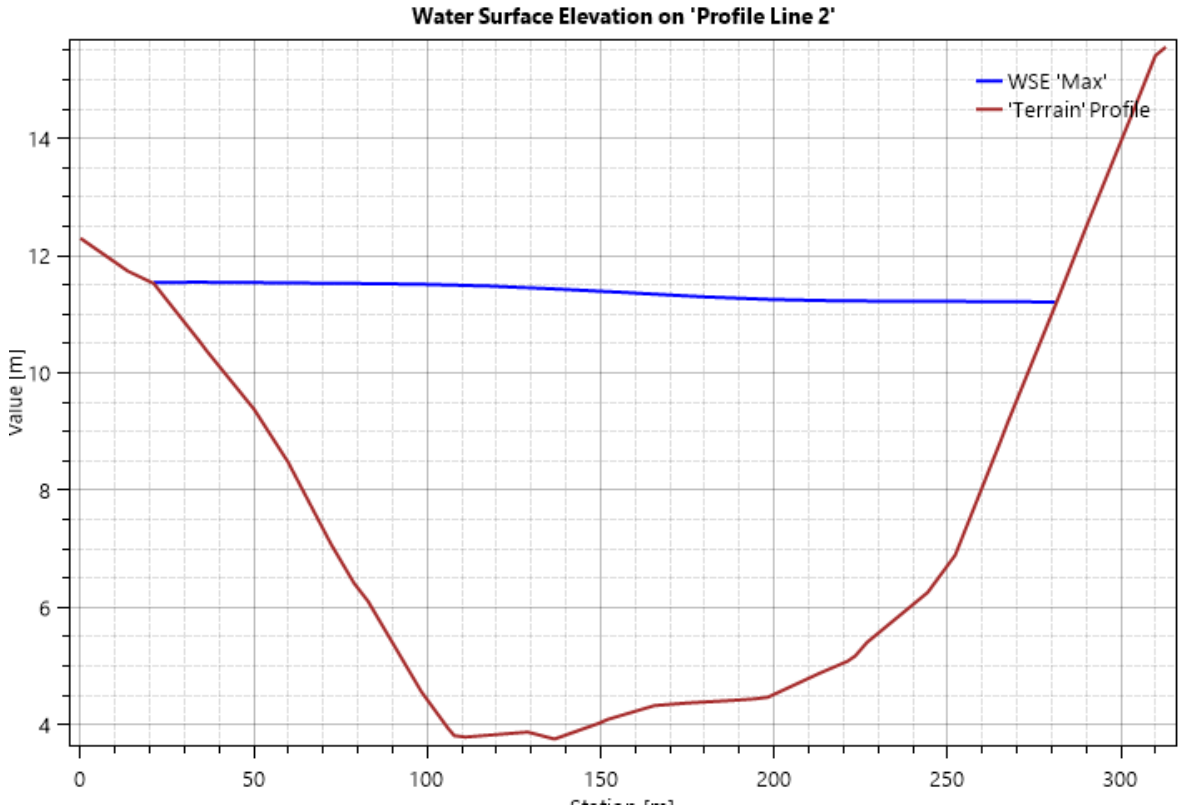

Figure B3: Profile line 3.